Monthly Notices
of the
ROYAL ASTRONOMICAL SOCIETY

Mon. Not. R. Astron. Soc. **399,** 2146–2164 (2009) doi:10.1111/j.1365-2966.2009.15416.x

The orbits of open clusters in the Galaxy

Zhen-Yu Wu,[1⋆] Xu Zhou,[1] Jun Ma[1] and Cui-Hua Du[1,2]

[1]*National Astronomical Observatories, Chinese Academy of Sciences, 20A Datun Road, Beijing 100012, China*
[2]*College of Physical Sciences, Graduate University of the Chinese Academy of Sciences, Beijing 100049, China*

Accepted 2009 July 17. Received 2009 July 17; in original form 2008 June 5

ABSTRACT

We present and analyse the kinematics and orbits for a sample of 488 open clusters (OCs) in the Galaxy. The velocity ellipsoid for our present sample is derived as $(\sigma_U, \sigma_V, \sigma_W) = (28.7, 15.8, 11.0)\,\mathrm{km\,s^{-1}}$ which represents a young thin-disc population. We also confirm that the velocity dispersions increase with the age of a cluster subsample. The orbits of OCs are calculated with three Galactic gravitational potential models. The errors of orbital parameters are also calculated considering the intrinsic variation of the orbital parameters and the effects of observational uncertainties. The observational uncertainties dominate the errors of derived orbital parameters. The vertical motions of clusters calculated using different Galactic disc models are rather different. The observed radial metallicity gradient of clusters is derived with a slope of $b = -0.070 \pm 0.011\,\mathrm{dex\,kpc^{-1}}$. The radial metallicity gradient of clusters based on their apogalactic distances is also derived with a slope of $b = -0.082 \pm 0.014\,\mathrm{dex\,kpc^{-1}}$. The distribution of derived orbital eccentricities for OCs is very similar to that derived for the field population of dwarfs and giants in the thin disc.

Key words: Galaxy: disc – Galaxy: kinematics and dynamics – open cluster and associations: general.

1 INTRODUCTION

Open clusters (OCs) have long been used as important tools in the study of the Galactic disc. The young clusters have been used to determine the spiral arm structure and to map the rotation curve of the Galaxy. The old clusters are excellent tracers of the structure, kinematics and chemistry of the Galactic disc (Friel 1995). In principle, basic parameters such as the distance, age and metallicity can be determined for a cluster more accurately than for a field star. Therefore, OCs are better tracers of large-scale properties of the Galactic disc population than field stars (Piskunov et al. 2006).

About 20 years ago, the catalogue of OC data compiled by Lyngå (1987) was used to derive the radial gradients and other structural properties of the Galactic disc (Lyngå 1982; Janes, Tilley & Lyngå 1988). In recent years, the available data on OCs have increased very quickly and the basic parameters of these clusters have also considerably improved. Dias et al. (2002, hereafter DAML) compiled a new catalogue of optically visible OCs and candidates including 1.5 times more clusters than the catalogue of Lyngå (1987). Kharchenko et al. (2005, hereafter K05) presented a catalogue of astrophysical data for 520 OCs, with data derived from the All-Sky Compiled Catalogue of 2.5 Million Stars (ASCC2.5; Kharchenko 2001). Using these data, the properties of the Galactic disc, such as the scaleheight, the scalelength and the metallicity distribution of the disc, were derived (Chen, Hou & Wang 2003; Bonatto et al. 2006; Piskunov et al. 2006).

⋆E-mail: zywu@bao.ac.cn

Lyngå & Palouš (1987) used 106 OCs with available data on positions, distances and radial velocities to analyse the local kinematics. They found that the dispersion of the radial velocity increases with age: for the old clusters it is about twice that of young clusters. Barkhatova, Kutuzov & Osipkov (1987, hereafter BKO) calculated the Galactic orbits for 69 OCs based on carefully selected data on distances, absolute proper motions and radial velocities. Keenan, Innanen & House (1973) calculated the orbits of NGC 188 and M67. In addition, Allen & Martos (1988) calculated the orbits for NGC 188, M67 and NGC 2420; Carraro & Chiosi (1994, hereafter C94) expanded the sample with five classic clusters and Finlay et al. (1995) calculated the orbits for a total of seven old clusters. Soubiran, Odenkirchen & Le Campion (2000) calculated the orbit for NGC 2355, de Oliveira et al. (2002) calculated the orbits for NGC 1912 and NGC 1907, and Wu et al. (2002) calculated the orbit for M48.

In recent years, Dias & Lépine (2005) determined the rotation velocity of the spiral pattern of the Galaxy by studying the birthplaces of OCs in the Galactic disc as a function of their ages. The birthplaces of these clusters were determined by assuming that their orbits were circular. Using 148 OCs within the projected distance on to the Galactic plane $d_{xy} \leq 0.85\,\mathrm{kpc}$, Piskunov et al. (2006) derived the solar motion and the velocity ellipsoid of OCs. They also calculated the Galactic orbits of these clusters and presented the mean parameters of their orbits. Based on the spatial and velocity distributions of OCs, Piskunov et al. (2006) also identified the existence of four open cluster complexes (OCCs) of different ages (Kharchenko & Piskunov 2006; Röser et al. 2007), which verified

the nature of clustering in OCs in the solar neighbourhood identified in previous studies (Efremov 1978; Éigenson & Yatsyk 1988; Barkhatova, Osipkov & Kutuzov 1989). Lépine, Dias & Mishurov (2008) used 374 OCs taken from the 2.7 version of the DAML catalogue to measure the epicycle frequency k in the Galactic disc. They also calculated the orbits of these OCs and discussed the distribution of the initial velocities of these clusters.

The orbital motions of OCs are important not only for our understanding of the dynamical evolution of OCs in the Galaxy (Friel 1999; Bergond, Leon & Guibert 2001), but also for investigating their effect on the time evolution of the abundance gradient in the Galactic disc (C94). The main aim of this paper is to calculate the orbits of OCs with the improved data for an enlarged sample of 488 OCs and to discuss the kinematical properties of these clusters.

We present the collection of data in Section 2. In Section 3, we analyse the statistical properties of the sample and especially their age–velocity dispersion relations. We present the orbital parameters and their associated uncertainties calculated in a given Galactic potential model in Section 4, followed by Section 5, which presents the differences of orbital parameters due to different Galactic potential models. In Section 6, we compare our results with the orbital parameters calculated for field stars and globular clusters, and discuss the effect of the orbital motions of OCs for the radial abundance gradient derived for these clusters; we also compare the orbital parameters with those derived by previous studies. Our conclusions are given in Section 7.

2 THE SAMPLE

2.1 The DAML catalogue

We chose the DAML catalogue as the main source of the fundamental parameters for the OCs. This catalogue uses the WEBDA data base[1] and previous catalogues of Lyngå (1987) as a starting point. Kinematical and metallicity data of the new objects when available are inserted (DAML). They also made use of the SIMBAD data base[2] and of the literature to find data on the clusters or on individual stars of the clusters, to obtain the averaged values of radial velocities and proper motions. This catalogue is regularly updated, and the latest version is available from its website.[3] The present 2.9 version (2008 April 13) of the DAML catalogue contains 1776 objects, of which 936 have published distances, ages and reddening values, 890 have published proper motions and 447 have radial velocities. 869 clusters with distances and proper motion data are taken from the DAML catalogue as the initial sample.

2.2 Distances

Most of the distances and ages listed in DAML are taken from WEBDA and are updated with new data from the literature (DAML). The distances estimated by Baumgardt, Dettbarn & Wielen (2000) based on *Hipparcos* parallaxes (ESA 1997) of member stars are also adopted by DAML. A comparison of the *Hipparcos* parallaxes with photometric distances shows good agreement (Baumgardt et al. 2000). The distances listed in DAML are taken from different authors using different observational techniques and reduction methods, and no errors for this parameter are listed in DAML; the non-uniformity and uncertainties in the adopted distance data should be estimated.

Paunzen & Netopil (2006) studied the accuracy of available parameters such as the age, reddening and distance for OCs by using the independently derived values published in the literature. They used a sample of 395 clusters in their statistical analysis. They found that, for about 80 per cent clusters in their sample, the error of distance is less than 20 per cent. They compared their results with the data of the DAML catalogue, and pointed out that the distances listed in the DAML catalogue have the same error distributions. In our present study, 20 per cent relative errors in distances are adopted for OCs in our sample.

van Leeuwen (2008) re-reduced the raw data of the *Hipparcos* mission, and the new reduction provides an improvement by a factor of 2.2 compared to the catalogue published in 1997 (van Leeuwen 2007). We calculate the difference between the distances derived by van Leeuwen (2008) using the re-reduced *Hipparcos* data and those listed in the DAML catalogue for a sample of 17 OCs in common. We get a difference of 6.2 ± 1.6 per cent between these two data sets, which is less than our adopted 20 per cent error for distance parameters and is considered in the following orbit calculation.

2.3 Absolute proper motions

The absolute proper motion data of OCs listed in DAML are adopted in the present study. The proper motion data are also compiled from different authors, but they are all based on the *Hipparcos* system. In our final sample, proper motions of 15 per cent clusters are derived from the *Hipparcos* catalogue (ESA 1997), 47 per cent proper motions are derived from the Tycho2 catalogue (Høg et al. 2000), 36 per cent proper motions are derived from the ASCC-2.5 catalogue (Kharchenko 2001) and only 2 per cent proper motions are derived from the Second US Naval Observatory CCD Astrograph Catalog (UCAC2) (Zacharias et al. 2004).

The *Hipparcos* catalogue is considered as the realization of the International Celestial Reference System (ICRS) at optical wavelengths. The systematic error of proper motions in the *Hipparcos* catalogue with respect to the ICRS is estimated to be 0.25 mas yr^{-1} (ESA 1997; Kovalevsky et al. 1997). Platais, Kozhurina-Platais & van Leeuwen (1998) searched the *Hipparcos* catalogue and found nine new OCs and derived the proper motions for these clusters. Baumgardt et al. (2000) determined the mean proper motions of 205 OCs from their member stars found in the *Hipparcos* catalogue. In our final sample, the proper motions derived from the *Hipparcos* catalogue are all taken from the results of Platais et al. (1998) and Baumgardt et al. (2000).

The Tycho2 catalogue (Høg et al. 2000) presents very precise proper motions with random errors between 1 and 3 mas yr^{-1} in the *Hipparcos* system. There are no significant systematic differences between the proper motions of these two catalogues (Urban, Wycoff & Makarov 2000). Dias, Lépine & Alessi (2001, 2002) determined the mean absolute proper motions of 206 OCs from the data in the Tycho2 catalogue. Alessi, Moitinho & Dias (2003) found 11 new OC candidates in the Tycho2 catalogue and determined the mean proper motions for these clusters. Loktin & Beshenov (2003) determined the mean proper motions for 167 OCs based on the kinematic and photometric data in the Tycho2 catalogue. Dias et al. (2001, 2002) compared their results with those derived by Baumgardt et al. (2000) based on the *Hipparcos* catalogue, and found that the mean difference in the proper motions is less than

[1] http://obswww.unige.ch/webda
[2] http://simbad.u-strasbg.fr/simbad/
[3] http://www.astro.iag.usp.br/∼wilton/

1 mas yr^{-1}. Loktin & Beshenov (2003) also compared their results with those derived by Dias et al. (2001), Dias et al. (2002b) and found that the difference is 4 ± 5 per cent. In our final sample, the mean proper motions derived from the Tycho2 catalogue are taken from the above-mentioned studies.

The ASCC-2.5 catalogue is based on large, modern, high-precision catalogues of the *Hipparcos*–Tycho family, including the Tycho2 catalogue, and provides the most complete all-sky catalogue of stars having uniform high-precision astrometric and photometric data down to $V \sim 14$ mag (Kharchenko 2001). In our final sample, the mean proper motions derived from the ASCC-2.5 catalogue by K05 and Kharchenko, Pakulyak & Piskunov (2003) are adopted. K05 and Kharchenko et al. (2003) compared their results with those derived by Baumgardt et al. (2000, 2001), Dias et al. (2002b) and found that their results agree quite well with previous studies.

The UCAC2 catalogue presents proper motions in the *Hipparcos* system with nominal errors of 1–3 mas yr^{-1} for stars up to $V \sim 12$ mag and about 4–7 mas yr^{-1} for fainter stars up to $V \sim 16$ mag. The systematic errors of the proper motions in UCAC2 are in the range 0.5–1.0 mas yr^{-1} (Zacharias et al. 2004). Dias et al. (2006) determined the mean proper motions for 428 OCs from the UCAC2 catalogue. They compared their results with those derived from the *Hipparcos* catalogue (Baumgardt et al. 2000), Tycho2 catalogue (Dias et al. 2001, 2002; Loktin & Beshenov 2003) and ASCC-2.5 catalogue (Kharchenko et al. 2003), and found that there is no statistical distinction among the compared mean proper motions of OCs in these catalogues.

We also calculate the difference of the mean proper motions derived by van Leeuwen (2008) using the re-reduced *Hipparcos* data and that adopted in our final sample taken from the DAML catalogue for the 17 OCs in common. We get a difference of 0.35 ± 0.22 mas yr^{-1} in $\mu_\alpha \cos\delta$ and a difference of 0.46 ± 0.43 in μ_δ. The differences are within the range of the errors for the mean proper motions listed in the DAML catalogue.

2.4 Radial velocities

There are 431 OCs whose distances, proper motions and radial velocities are available from the DAML catalogue. Most radial velocities are taken from the catalogues compiled by K05 and Kharchenko et al. (2007). K05 cross-identified the ASCC-2.5 catalogue with the General Catalogue of Radial Velocities of Barbier-Brossat & Figon (2000) and derived radial velocities for 290 OCs based on their membership determination. They found that the mean difference between their results and those in the published literature for common clusters is 0.36 ± 0.88 km s^{-1}. The 363 radial velocities of OCs compiled by Kharchenko et al. (2007) are derived from the second version of the Catalogue of Radial Velocities of Galactic stars with high-precision Astrometric Data (CRVAD-2). The CRVAD-2 is the result of updating and expanding the list of stars with known radial velocities and high-precision astrometric and photometric data taken from the ASCC-2.5 catalogue. The mean difference of radial velocities for 177 clusters in common between the CRVAD-2 and the literature is 0.65 ± 0.72 km s^{-1}.

Frinchaboy & Majewski (2008) presented high-precision radial velocities for 71 OCs obtained with multi-object spectrographs. For 25 clusters in their sample, the radial velocities are newly obtained and are not included in DAML. Mermilliod, Mayor & Udry (2008) derived mean radial velocities for 166 OCs based on observations with the Correlation Radial Velocity (CORAVEL) spectrovelocimeters. The radial velocities of 64 OCs derived by Mermilliod et al. (2008) are not listed in DAML.

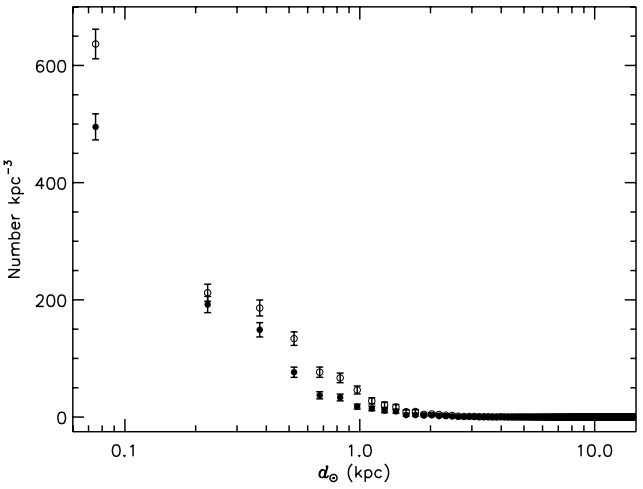

Figure 1. The volume density distributions of OCs as a function of their heliocentric distance $d_\odot$. The open circles represent the OCs in the DAML catalogue with distance data available and the filled circles represent the OCs in our present sample.

We supplement the new radial velocities derived by Frinchaboy & Majewski (2008) and Mermilliod et al. (2008) into our final sample. We also update the known radial velocities in DAML with those derived by Mermilliod et al. (2008) due to their higher precision.

In our final sample, 488 OCs with distances, proper motions and radial velocities are included.

2.5 Completeness of the present sample

Our present sample is a subsample mainly taken from the DAML catalogue. We plot the volume density of 1082 OCs (open circles) with distance data available in DAML as a function of the heliocentric distance $d_\odot$ in Fig. 1. In order to estimate the completeness of the OCs in our present sample, we also plot the volume density of 488 OCs (filled circles) in our present sample in Fig. 1. For clusters with heliocentric distance $d_\odot > 2.0$ kpc, the volume density distributions for these two samples of OCs are completely consistent. For clusters with heliocentric distance $d_\odot < 2.0$ kpc, the volume densities of OCs in our present sample are less than those for OCs in DAML, but the distributions for these two samples are very similar. Fig. 1 indicates that our present sample of OCs is a representative subsample of currently observed OCs in the Galaxy.

Using a sample of 654 OCs with distance data available, Bonatto et al. (2006) simulated the effects of completeness in their sample of OCs. They found that a total number of ∼730 OCs with heliocentric distance $d_\odot \leq 1.3$ kpc should be observed. Within the same distance range, there are 498 OCs in the DAML catalogue and 271 OCs in our present sample; the completeness can be estimated as 68 per cent and 37 per cent for the DAML catalogue and for our present sample, respectively. A possible source for the rest of the unobserved OCs comes from the very young clusters which are still embedded within giant molecular clouds; they are heavily obscured and are very difficult to identify (Lada & Lada 2003).

2.6 Initial conditions

Table 1 lists the adopted positions (α, δ), heliocentric distances $d_\odot$, radial velocities v_r and absolute proper motions ($\mu_\alpha \cos\delta$,

Table 1. The observed data of 488 OCs in our sample. The full version of this table is available in the online version of the article (see Supporting Information).

Name	α(2000.0) h m s	δ(2000.0) ° ′ ″	$d_\odot$ (kpc)	v_r (km s^{-1})	$\mu_\alpha \cos\delta$ (mas yr^{-1})	μ_δ (mas yr^{-1})	Age (Myr)	[Fe/H]
Berkeley 59	00 : 02 : 14	+67 : 25 : 00	1.000 ± 0.200	−12.5 ± 7.1	−2.11 ± 0.81	−1.20 ± 0.75	6.3	
Blanco 1	00 : 04 : 07	−29 : 50 : 00	0.269 ± 0.054	4.1 ± 1.4	20.17 ± 0.51	3.00 ± 0.51	62.5	0.04
Alessi 20	00 : 09 : 23	+58 : 39 : 57	0.450 ± 0.090	−11.5 ± 0.0	8.73 ± 0.53	−3.11 ± 0.53	166.0	
ASCC 1	00 : 09 : 36	+62 : 40 : 48	4.000 ± 0.800	−69.7 ± 4.7	−2.07 ± 0.72	0.46 ± 0.57	177.8	
Mayer 1	00 : 21 : 54	+61 : 45 : 00	1.429 ± 0.286	−20.9 ± 2.0	−4.46 ± 1.13	−6.66 ± 0.94		
NGC 129	00 : 30 : 00	+60 : 13 : 06	1.625 ± 0.325	−39.4 ± 0.5	−1.06 ± 0.94	1.60 ± 0.94	76.9	
ASCC 3	00 : 31 : 09	+55 : 16 : 48	1.700 ± 0.340	−37.0 ± 0.0	−1.92 ± 0.61	−1.25 ± 0.59	79.4	
NGC 225	00 : 43 : 39	+61 : 46 : 30	0.657 ± 0.131	−28.0 ± 0.0	−4.95 ± 0.76	−0.50 ± 0.76	130.0	
NGC 188	00 : 47 : 28	+85 : 15 : 18	2.047 ± 0.409	−45.0 ± 10.0	−1.48 ± 1.25	−0.56 ± 1 .24	4285.5	−0.01
IC 1590	00 : 52 : 49	+56 : 37 : 42	2.940 ± 0.588	−32.5 ± 6.4	−1.36 ± 0.23	−1.34 ± 0.83	3.5	
–	–	–	–	–	–	–	–	–
–	–	–	–	–	–	–	–	–

μ_δ) of 488 OCs in our final sample. The adopted 20 per cent errors for distances, the errors of absolute proper motions and of radial velocities listed in DAML, Frinchaboy & Majewski (2008) and Mermilliod et al. (2008), respectively, are also presented in Table 1. In Table 1, we also list the ages and metallicities [Fe/H] for each cluster if available in DAML. Ages are currently available for 445 OCs, 109 of which have [Fe/H] values that are also available.

The initial conditions for orbit calculation are the presently observed positions and velocities of OCs with respect to the galactocentric reference frame. Adopting the solar motion $(U, V, W)_\odot = (10.0, 5.2, 7.2)$ km s^{-1} from Dehnen & Binney (1998), the local standard of rest (LSR) velocities of OCs are determined from the data listed in Table 1. The LSR velocities are then corrected to the Galactic standard of rest (GSR) by adopting the galactocentric distance of Sun $R_\odot = 8.0$ kpc (Reid 1993) and a rotation velocity of the LSR of 220 km s^{-1} (Kerr & Lynden-Bell 1986). All space coordinates x, y, z and velocity components U, V, W refer to a galactocentric right-handed Cartesian coordinate system with the x direction directed towards the Galactic anticentre and the z direction directed towards the Galactic North Pole (Odenkirchen & Brosche 1992). The U, V, W velocity components and their errors are calculated with the method of Johnson & Soderblom (1987). Table 2 lists the initial conditions used to calculate the orbital solution for each cluster in our sample. The errors in velocity components include the errors in absolute proper motions, radial velocities and distances of OCs listed in Table 1.

3 PARAMETER DISTRIBUTIONS AND KINEMATICS OF THE SAMPLE

3.1 Parameter distributions of the present sample

Fig. 2 shows the distributions of ages, metallicities [Fe/H] and observed galactocentric distances R_{GC} of OCs in our present sample. Due to the large difference among the ages of OCs, the distributions of age are plotted in panels (a) and (b) of Fig. 2. We can see from panels (a) and (b) of Fig. 2 that about two-third OCs have ages less than 100 Myr. The oldest cluster has an age of 9.0 Gyr. No clusters in our sample have been found to be in the age interval 0.9–1.0 Gyr. The distribution of metallicities [Fe/H] of OCs is plotted in panel (c) of Fig. 2. Except for two clusters with [Fe/H] < -0.5, the distribution of [Fe/H] can be fitted by two Gaussian functions. For clusters with $-0.5 <$ [Fe/H] < -0.2, the [Fe/H] data can be fitted by a Gaussian function with mean $\mu_{[Fe/H]} = -0.31$ and dispersion $\sigma_{[Fe/H]} = 0.07$; for clusters with [Fe/H] > -0.2, the best-fitting Gaussian function has mean $\mu_{[Fe/H]} = 0.0$ and dispersion $\sigma_{[Fe/H]} = 0.13$. It should be noted that the sample of clusters with [Fe/H] data is very incomplete; the distribution of [Fe/H] in panel (c) of Fig. 2 may not be the true distribution of the metallicities for the complete

Table 2. The present positions and velocities of 488 OCs in our sample. The full version of this table is available in the online version of the article (see Supporting Information).

Name	x	y (kpc)	z	U	V (km s^{-1})	W
Berkeley 59	−8.471 ± 0.094	0.878 ± 0.176	0.087 ± 0.017	25.3 ± 5.1	219.7 ± 6.6	2.4 ± 0.7
Blanco 1	−7.952 ± 0.010	0.013 ± 0.003	−0.264 ± 0.053	−13.4 ± 4.9	217.1 ± 1.8	−1.7 ± 0.7
Alessi 20	−8.207 ± 0.041	0.398 ± 0.080	−0.030 ± 0.006	0.2 ± 3.2	206.5 ± 1.8	−1.6 ± 0.2
ASCC 1	−9.887 ± 0.377	3.527 ± 0.705	0.014 ± 0.003	75.8 ± 13.9	181.3 ± 8.4	21.9 ± 0.3
Mayer 1	−8.702 ± 0.141	1.244 ± 0.249	−0.023 ± 0.005	51.2 ± 9.1	223.7 ± 5.3	−33.8 ± 0.5
NGC 129	−8.818 ± 0.164	1.402 ± 0.280	−0.072 ± 0.014	35.7 ± 6.4	195.3 ± 3.9	21.9 ± 0.7
ASCC 3	−8.843 ± 0.169	1.459 ± 0.292	−0.221 ± 0.044	43.0 ± 5.2	200.6 ± 3.0	3.3 ± 0.0
NGC 225	−8.348 ± 0.069	0.557 ± 0.111	−0.012 ± 0.002	38.0 ± 3.3	209.6 ± 2.1	6.6 ± 0.4
NGC 188	−9.027 ± 0.205	1.590 ± 0.318	0.780 ± 0.156	43.6 ± 11.8	199.7 ± 1.0	−14.7 ± 0.8
IC 1590	−9.597 ± 0.319	2.448 ± 0.490	−0.320 ± 0.064	44.6 ± 5.6	206.7 ± 6.0	−7.9 ± 0.1
–	–	–	–	–	–	–
–	–	–	–	–	–	–

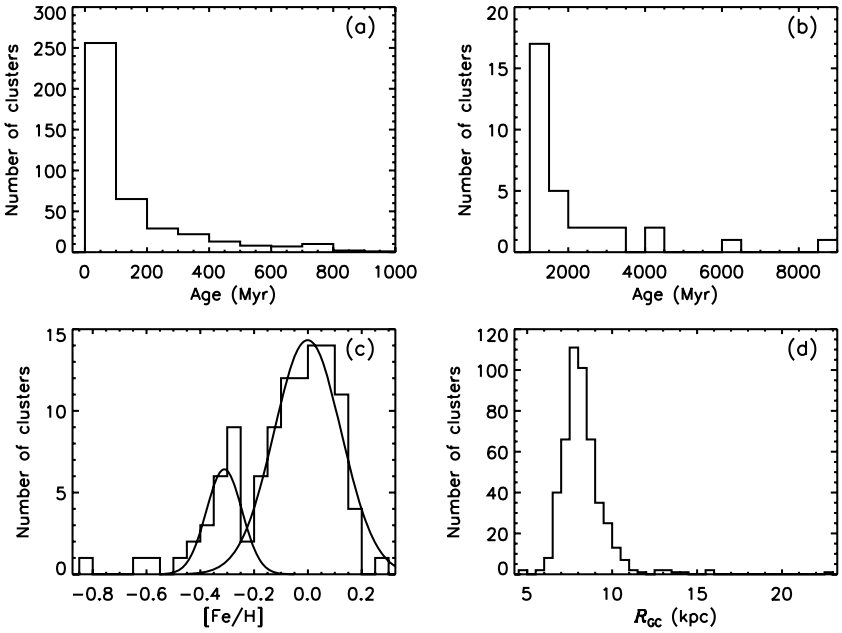

Figure 2. Distributions of ages, metallicities [Fe/H] and observed galactocentric distances R_{GC} of OCs in our present sample.

sample of OCs in the Galaxy. From panel (d) of Fig. 2, it can be seen that most OCs distribute near the Sun. The minimum and maximum galactocentric distances of OCs in our present sample are 4.6 and 22.6 kpc, respectively.

3.2 Age–velocity dispersion relations

In recent years, much observational efforts have been devoted to constrain the age–velocity dispersion relation of the thin disc. Nordström et al. (2004, hereafter N04) presented new determinations of metallicity, age, kinematics and Galactic orbits for a complete, magnitude-limited and kinematically unbiased sample of ∼14 000 F and G dwarf stars near the solar neighbourhood. The *Hipparcos*/Tycho-2 parallaxes and proper motions, together with some 63 000 new, accurate radial velocity observations supplemented by a few earlier radial velocities, were used to compute the space velocity components and their dispersions. Ages and their errors were computed from a set of theoretical isochrones by a sophisticated Bayesian technique (Jørgensen & Lindegren 2005). N04 found that the age–velocity dispersion relations of each space velocity component can be fitted by continuous smooth power laws: $\sigma \propto \mathrm{age}^k$, which also evidences the continuous heating of the disc in all directions.

Holmberg, Nordström & Andersen (2007) redetermined the basic calibrations used to infer astrophysical parameters for the N04 stars from *uvby* photometry. Using the improved astrophysical parameters, they recomputed the ages and age error estimates for the N04 sample. Based on their revised data set, and with substantially higher time resolution than that in the original N04, Holmberg et al. (2007) confirmed the conclusion of N04 that the dynamical heating of the thin disc continues throughout its life.

Seabroke & Gilmore (2007) revisited the Galactic thin-disc age–velocity dispersion relation based on the N04 sample; their new result is that a power law is not required by the data of N04, and disc heating models that saturate after ∼4.5 Gyr are equally consistent with the observations.

Soubiran et al. (2008, hereafter S08) presented the parameters of 891 stars, mostly local and distant clump giants, including distances, absolute magnitudes, spatial velocities, galactic orbits and ages. Using their distant sample of clump giants, and rejecting stars having a probability higher than 80 per cent of belonging to the thick disc, the Hercules stream and the halo, S08 found that the velocity dispersions in V and W saturate at ∼4 Gyr and the dispersion in U increases smoothly with time.

Using radial velocities of 67 clusters within 2 kpc from the Sun, Lyngå & Palouš (1987) found that the dispersion of the radial velocity increases with age. Based on proper motions and distances of 148 clusters within the projected distance on to the Galactic plane $d_{xy} \leq 0.85$ kpc from the Sun, Piskunov et al. (2006) derived the tangential velocity dispersions for clusters with different ages and also found that the dispersions increase with age.

The OCs in our sample with errors in the spatial velocities less than 20 km s^{-1} are used to derive the velocity dispersion in each velocity component. Those clusters are divided into three age groups: $0 < \mathrm{age} \leq 500$ Myr, $500 < \mathrm{age} \leq 1000$ Myr and $1000 < \mathrm{age} \leq 2000$ Myr. For each age group, the velocity dispersion in each velocity component U, V and W is calculated. The number N of clusters in each age group is also listed in Table 3. Table 3 indicates that the velocity dispersions in the U and W components in the age group of $500 < \mathrm{age} \leq 1000$ Myr are only marginally larger than those in the age group with age <500 Myr, but the velocity dispersions in all of the three velocity components in the age group with age > 1 Gyr are larger than those for the clusters with age < 1 Gyr.

Table 3. Age–velocity dispersion relations derived from OCs in our present sample with errors in the spatial velocities less than 20 km s^{-1}.

Age (Myr)	σ_U	σ_V	σ_W	N
Age ≤ 500	28.3	15.4	10.6	339
500 < Age ≤ 1000	29.1	13.8	11.9	25
1000 < Age ≤ 2000	31.7	23.4	17.7	16

The velocity dispersions in our present sample of OCs indicate the continuous dynamical heating of the thin disc.

Using OCs with errors in the spatial velocities less than 20 km s^{-1} in our present sample, the velocity dispersions are derived as (σ_U, σ_V, σ_W) = (28.7, 15.8, 11.0) km s^{-1}. The derived velocity dispersions are smaller than those for the thin-disc clump giants (σ_U, σ_V, σ_W) = (41.5, 26.4, 22.1) km s^{-1} derived by S08. For their subsample of clump giants with an age of 1.5 Gyr, S08 derived the velocity dispersions as (σ_U, σ_V, σ_W) = (36.2, 19.9, 18.7) km s^{-1}, which are close to our results for OCs with age > 1 Gyr. So, the main reason for the difference between the velocity dispersions for OCs in our present sample and those for the giants of S08 is that in our present sample of OCs, most of them are young clusters with an age less than 1 Gyr. The giants sample of S08 represents an old thin disc; most of the giants in their sample are older than 1 Gyr. Just as we have pointed out in the previous section, the thin disc of the Galaxy is continuously heated, so the velocity dispersions for a young population such as the OCs in our present sample should be less than those corresponding to an older population such as the giants sample of S08.

Using OCs within the projected distance on to the Galactic plane $d_{xy} \leq 0.85$ kpc from the Sun, Piskunov et al. (2006) derived the velocity dispersions as (σ_U, σ_V, σ_W)=(13.86, 8.75, 5.05) km s^{-1}, which are smaller than those derived from our present sample. Piskunov et al. (2006) used a volume-limited sample of relatively young clusters; in contrast, our present sample includes many older clusters and also objects located further away. Therefore, our larger velocity dispersions reflect the effects of dynamical heating of the thin disc. Using the clusters in our present sample within the projected distance on to the Galactic plane $d_{xy} \leq 0.85$ kpc, we derive the velocity dispersions as (σ_U, σ_V, σ_W) = (16.8, 9.6, 5.3) km s^{-1}, which are close to the results of Piskunov et al. (2006).

4 ORBITAL PARAMETERS AND THEIR UNCERTAINTIES

4.1 The Galactic gravitational potential model

In this study, we employ the axisymmetric Galactic gravitational potential model of Allen & Santillán (1991, hereafter AS91). This model consists of a spherical central bulge and a disc in the form proposed by Miyamoto & Nagai (1975), plus a massive, spherical halo extending to a radius of 100 kpc from the centre of the Galaxy. The total mass of the model is 9.0×10^{11} M$_\odot$ and the local total mass density at the solar position is $\rho_0 = 0.15$ M$_\odot$ pc^{-3}. The rotation curve of this potential represents the current knowledge of galactic rotation in the Galaxy. This model is time independent, completely analytical and very simple. The integration of the orbit, using this model, is very rapid and can achieve high numerical precision. The potential admits two conserved quantities: the total energy E and the z-component J_z of the angular momentum vector. This model has been used to derive the galactic orbits of OCs (C94), globular clusters (hereafter A06, A08, respectively Odenkirchen et al. 1997; Allen, Moreno & Pichardo 2006; Allen, Moreno & Pichardo 2008) and clump giants near the Sun (S08).

4.2 The orbital parameters

Using the data listed in Table 2, the orbits are calculated backwards in time over an interval of 5 Gyr. Most clusters in our sample have ages less than 100 Myr; they do not even move one galactic orbit in the Galaxy. The integration time is chosen to ensure that clusters can move more galactic orbits in the Galaxy and the averaged orbital parameters can be determined. For the integration, we use the Bulirsch–Stoer algorithm of Press et al. (1992). The relative change in the total energy over the 5 Gyr integration time is of the order of 10^{-14}–10^{-15}.

The orbital parameters are listed in Table 4. R_a and R_p are apogalactic and perigalactic distances from the Galactic centre, respectively, which are determined from the averaged maximum and minimum galactocentric distances of the cluster in the calculated Galactic orbit within the integration time of 5 Gyr. The orbital eccentricity e is calculated as $e = (R_a - R_p)/(R_a + R_p)$, where R_a and R_p are averages. The maximum distance above the Galactic plane, z_{max}, is also the averaged maximum vertical distances above the Galactic plane in the cluster's orbit within the given integration time. T_p is the orbital period defined as the period of revolution around the z-axis. T_z is the mean time interval of the cluster to cross the Galactic plane from one z_{max} to the other in the opposite direction. Because of the right-handed orientation of the coordinate system adopted here, the negative J_z of the z-component of the angular momentum vector corresponds to prograde rotation in the Galaxy and vice versa (Odenkirchen et al. 1997).

In Fig. 3, we plot the distributions of derived orbital parameters. In the panels of z_{max}, T_p and T_z, some very large values are not plotted. The distributions of R_a, R_p, T_p and T_z are fitted by Gaussian functions $\sim e^{-(x-\mu)^2/2\sigma^2}$ and the distributions of e and z_{max} are fitted

Table 4. The orbital parameters and their errors of 488 OCs in our sample calculated with the AS91 model. The full version of this table is available in the online version of the article (see Supporting Information).

Name	R_a (kpc)	R_p (kpc)	e	z_{max} (kpc)	T_p (Myr)	T_z (Myr)	J_z (kpc km s^{-1})
Berkeley 59	8.6 ± 0.4	8.5 ± 0.3	0.01 ± 0.03	0.09 ± 0.02	239.3 ± 8.4	35.1 ± 1.6	−1883.3 ± 65.2
Blanco 1	8.2 ± 0.1	7.5 ± 0.2	0.05 ± 0.02	0.26 ± 0.05	221.1 ± 1.3	36.4 ± 1.3	−1726.2 ± 16.8
Alessi 20	8.3 ± 0.1	7.2 ± 0.1	0.07 ± 0.02	0.03 ± 0.01	217.0 ± 0.6	30.8 ± 0.3	−1694.8 ± 8.5
ASCC 1	10.6 ± 0.8	8.5 ± 1.2	0.11 ± 0.05	0.33 ± 0.26	268.5 ± 27.3	46.5 ± 11. 9	−2059.9 ± 209.0
Mayer 1	10.0 ± 0.9	8.5 ± 0.3	0.08 ± 0.03	0.50 ± 0.24	261.8 ± 16.5	50.0 ± 10. 1	−2010.3 ± 94.4
NGC 129	8.9 ± 0.2	7.4 ± 0.4	0.10 ± 0.02	0.28 ± 0.12	229.3 ± 7.8	38.5 ± 4.5	−1772.2 ± 64.7
ASCC 3	9.0 ± 0.2	7.8 ± 0.4	0.07 ± 0.02	0.21 ± 0.04	235.6 ± 8.3	37.7 ± 2.5	−1836.6 ± 67.5
NGC 225	8.8 ± 0.2	7.4 ± 0.2	0.09 ± 0.01	0.07 ± 0.03	227.7 ± 4.5	33.3 ± 0.8	−1770.9 ± 35.5
NGC 188	9.3 ± 0.6	8.1 ± 0.8	0.07 ± 0.04	0.79 ± 0.21	246.7 ± 17.3	57.1 ± 8.8	−1872.0 ± 129.0
IC 1590	10.0 ± 0.6	9.2 ± 0.6	0.04 ± 0.02	0.33 ± 0.17	268.7 ± 17.0	46.5 ± 8.1	−2092.9 ± 119.8
–	–	–	–	–	–	–	–
–	–	–	–	–	–	–	–

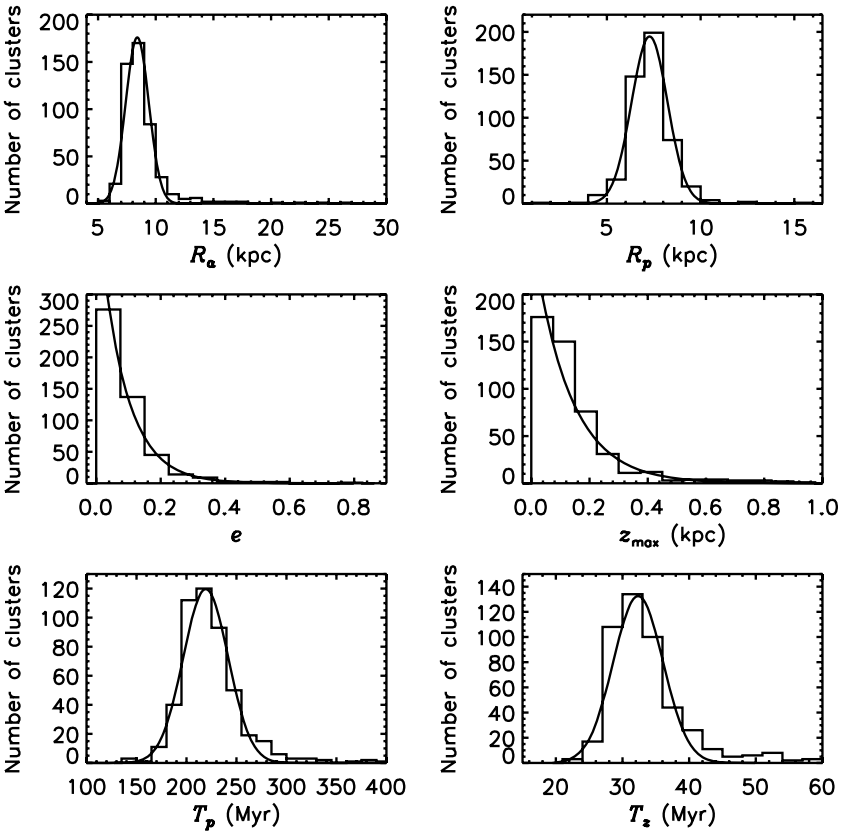

Figure 3. Distributions of derived orbital parameters calculated with the AS91 model for OCs in our present sample.

by exponential functions $\sim e^{-x/\beta}$. The means and dispersions of the Gaussian functions for R_a, R_p, T_p and T_z are derived as $\mu_{R_a} = 8.40$ and $\sigma_{R_a} = 1.00$ kpc, $\mu_{R_p} = 7.28$ and $\sigma_{R_p} = 0.96$ kpc, $\mu_{T_p} = 219.3$ and $\sigma_{T_p} = 22.5$ Myr, and $\mu_{T_z} = 32.3$ and $\sigma_{T_z} = 3.7$ Myr, respectively. The parameters β for the distributions of e and z_{max} are derived as $\beta_e = 0.08$ and $\beta_{z_{max}} = 0.13$. The derived parameter β and Fig. 3 show that, for most of the OCs, the orbital eccentricities e are less than 0.1 and z_{max} less than 200 pc. In our sample, the minimum of R_p is bigger than 1 kpc and the mean of R_p is $\sim$7.0 kpc. Therefore, the orbits of OCs in our present sample cannot be noticeably affected by a barred mass distribution in the Galactic centre within 1 kpc (Dinescu, Girard & van Altena 1999; A06). Fig. 3 also indicates that, in one orbital period, most of the clusters can cross the Galactic plane seven times.

As a representative example, a few of the orbits calculated with the AS91 model in a time interval of 2 Gyr are presented in Fig. 4. For each cluster, the panel on the left shows the orbit projected on to the Galactic plane, while the panel on the right shows the meridional orbit. The filled square indicates the present observed position for each cluster. The orbits of NGC 188, NGC 2682, NGC 2420, NGC 752 and NGC 2506 are also calculated by C94 and Finlay et al. (1995). For other clusters presented in Fig. 4, Berkeley 33 has a maximum of $R_a = 48.3$ kpc, Berkeley 20 has a maximum eccentricity $e = 0.81$, Berkeley 29 and Berkeley 31 have the maximum values of z_{max} and NGC 6791 is amongst the most massive OCs known today (Friel 1999).

All of the meridional orbits in Fig. 4 are of a boxy-like type. Clusters move in the meridional plane within the limited areas almost filling the boxes symmetrically. But the meridional orbits of Berkeley 33 and Berkeley 20 are not symmetric with respect to the Galactic plane. The orbits projected on the Galactic plane in Fig. 4 indicate the periodic motions of clusters more clearly.

4.3 The errors in the orbital parameters

The errors for the derived orbital parameters listed in Table 4 include two types of uncertainties affecting the derived results. The first one is the intrinsic variation of the orbital parameters within the 5 Gyr integration interval. The dispersions of the averaged orbital parameters are calculated over the number of galactic orbits, which indicate the intrinsic nature of the orbit, and this may be due to effects from chaos, and/or a complex distribution of orbit families (Dinescu et al. 1999).

On the other hand, the main errors of the orbital parameters come from the observational uncertainties of the input data. In the input data, a 20 per cent relative error is assumed for distance, the median of the relative errors in radial velocities is about 6 per cent and the median of the relative errors in proper motions is 23 per cent. The uncertainties in distance and proper motions are the main sources for the errors in the derived orbital parameters. The effects of observational uncertainties cannot be simply propagated into the derived orbital parameters (Odenkirchen & Brosche 1992). Following Dinescu et al. (1999), the initial conditions are generated in a Monte Carlo fashion by adding Gaussian deviates to the observed absolute proper motions, radial velocities and distances. The standard deviations are taken to be the errors for the input data listed in Table 1. For each cluster, the errors for its orbital parameters have been calculated based on 1000 separate integrations.

Compared with the uncertainties in the derived orbital parameters due to the errors in the input data, the intrinsic uncertainties of

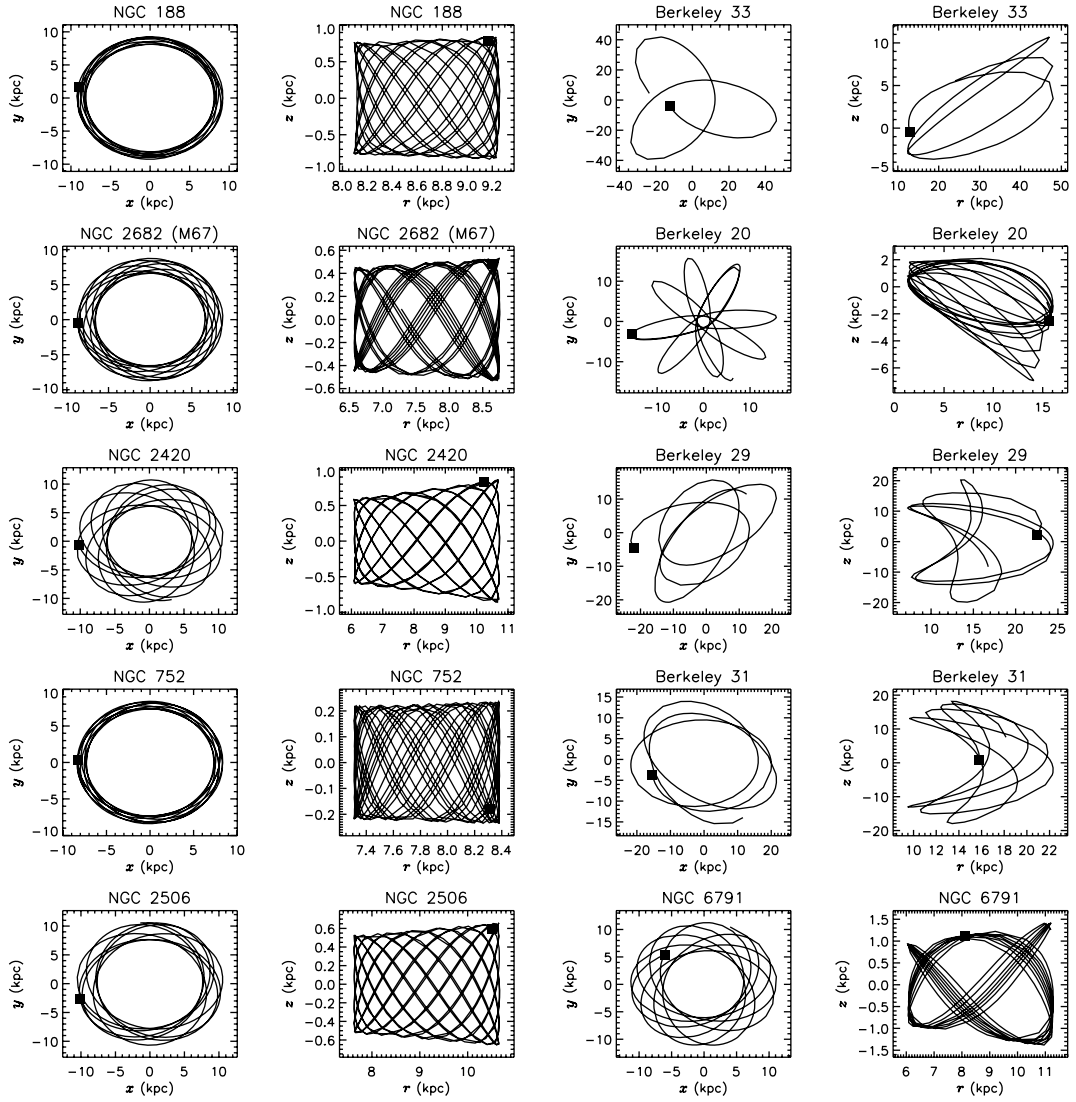

Figure 4. Meridional Galactic orbits and orbits projected on to the Galactic plane in the time interval of 2 Gyr for some OCs calculated with the AS91 model. The filled square shows the present observed position for each cluster.

Table 5. The relative error percentages of derived orbital parameters due to observational uncertainties and the relative difference percentages of derived orbital parameters by different Galactic potential models.

Parameter	Observational uncertainty (per cent)	P90 (per cent)	FSC96 (per cent)
R_a	2.9	0.0	0.2
R_p	3.5	0.5	0.3
e	27.5	0.0	0.0
z_{max}	43.3	1.1	21.2
T_p	2.8	0.8	1.5
T_z	3.9	2.9	31.5

the orbits within the given integration interval are very small. For each cluster, considering only the observational errors of the input data, the relative errors in the derived orbital parameters are also calculated. For each orbital parameter, the median of the relative errors for this parameter is calculated and listed as percentage in column 2 of Table 5. Table 5 shows that the uncertainties of orbital eccentricity e and the maximum distance from the Galactic plane z_{max} are much more affected by the observational errors. The large uncertainty of e is propagated from the uncertainties of both R_a and R_p. The reason for the large uncertainty of z_{max} is that, for most of the OCs, they move near the Galactic disc and have small vertical distances from the Galactic plane, so small changes in input data produce big relative changes of their orbits in the direction perpendicular to the disc.

4.4 The effect of adopting different observational errors in input data on the derived orbital parameters

Comparing the observational errors in the input data, the relative error in radial velocity is smaller than that in proper motion and distance. The errors in the derived orbital parameters are dominated by the observational errors in proper motions and distances. In order to estimate the effect of different observational accuracy in proper motions and distances on the derived orbital parameters, we repeated the Monte Carlo procedure mentioned above. We assumed 50 per cent and 80 per cent relative errors for the adopted proper motion and distance data, respectively. We also assumed 50 per cent

Table 6. The relative error percentages of derived orbital parameters for adopted different observational uncertainties in proper motions μ and distances from the Sun $d_\odot$.

Parameter	Observational uncertainty					
	50 per cent in μ	80 per cent in μ	50 per cent in $d_\odot$	80 per cent in $d_\odot$	50 per cent in μ+$d_\odot$	80 per cent in μ+$d_\odot$
R_a	3.9	4.8	6.8	11.5	7.5	14.5
R_p	5.0	5.8	6.7	9.9	7.7	12.6
e	45.0	54.4	45.0	62.5	61.4	102.2
z_{max}	76.8	112.9	81.5	130.0	121.0	271.7
T_p	3.7	4.3	5.8	9.7	6.5	12.3
T_z	6.3	11.7	8.3	14.9	11.1	26.2

and 80 per cent relative errors for both proper motion and distance all together.

There are six sets of simulations. In each set of simulation, except for the assumed different relative errors for proper motions or distances, the errors for other input data are the same as those considered in the previous section. For each set of simulations, we calculated the relative error for each orbital parameter; the medians of the relative errors are listed in Table 6. Table 6 indicates that the relative errors in e and z_{max} increase obviously with the increase of errors in input data. The uncertainties of e and z_{max} are very sensitive to the errors in the input data just as Table 5 has indicated. Table 6 also shows that, assuming the same relative error for proper motion and distance, the relative errors in the derived orbital parameters caused by the error of distance are bigger than those caused by the error of proper motion.

5 ORBITAL PARAMETERS IN DIFFERENT GALACTIC POTENTIAL MODELS

We use two different potential models to calculate the differences in the derived orbital parameters. The first model is the one proposed by Paczyński (1990, hereafter P90) and then used by Dinescu et al. (1999) as their representative model for calculating the orbits of 38 globular clusters. This model consists of axisymmetric potential with three components: bulge, disc and dark halo. The bulge is modelled as the Plummer potential (Plummer 1911). The disc is the same as AS91 in the form of Miyamoto & Nagai (1975) with different coefficients. The dark halo is modelled as logarithmic potential, which assures a flat rotation curve, but implies an infinite mass.

The second model is the one proposed by Flynn, Sommer-Larsen & Christensen (1996, hereafter FSC96) and used by N04 to calculate the orbits of nearby F and G dwarf stars. This axisymmetric potential also consists of three components: central core, disc and dark halo. The potential of the central core is modelled by two spherical components, representing the bulge/stellar halo and an inner core component. The disc is modelled using a combination of three analytical discs of Miyamoto & Nagai (1975). The potential of the dark halo is assumed to be logarithmic.

In Figs 5 and 6, we compare the orbital parameters derived from P90 and FSC96 models with those derived from the AS91 model. Fig. 5 shows that the orbital parameters derived from the P90 model are very consistent with those derived from the AS91 model, and no systematic differences can be found. For the FSC96 model, Fig. 6 shows that R_p and e are consistent between FSC96 and AS91 models, and there are no systematic differences in these two parameters. But for $R_a > 15$ kpc, R_a and T_p derived for the FSC96 model are systematically smaller than those derived from the AS91 model. Fig. 6 also indicates that z_{max} and T_z derived for the FSC96 model are systematically bigger than those derived from the AS91 model.

In Figs 7 and 8, for P90 and FSC96 models, we show the orbits for the same clusters as presented in Fig. 4. Fig. 7 indicates that the orbital shapes for most of the clusters, including the asymmetric meridional orbits of Berkeley 33 and Berkeley 20, are very similar between P90 and AS91 models. Fig. 8 shows that for most of the clusters, the orbital shapes derived from the FSC96 model are different from those derived from the AS91 model. The meridional orbits of Berkeley 33 and Berkeley 20 are symmetric in the FSC96 model.

For each cluster, the relative difference in each orbital parameter from different models is calculated as $(P_{(P90orFSC96)} - P_{AS91})/P_{AS91}$, where P_{P90}, P_{AS91} and P_{FSC96} represent the derived orbital parameters by P90, AS91 and FSC96 models, respectively. For each orbital parameter, the median of the relative difference between the given models and AS91 model is listed in Table 5. Table 5 shows that the relative differences of the derived orbital parameters for the P90 model are smaller than those for the FSC96 model. Especially for z_{max} and T_z, the results derived from the FSC96 model are very different from those derived from AS91 and P90 models. The consistent orbital parameters derived from AS91 and P90 models are due to the very similar mass distributions of these two models. The main difference between AS91 and P90 models is the bulge model, whereas the bulge model dominates the orbit of a cluster only within 1 kpc from the Galactic centre. No clusters in our present sample can move to this range. The FSC96 model is very different from AS91; the total mass interior to the same galactocentric distance R in the FSC96 model is much larger than that in the AS91 model when $R > 10$ kpc. The larger mass of the FSC96 model can control the cluster to move within a smaller apogalactic distance. On the other hand, the mass of the disc in the FSC96 model is smaller than that in the AS91 model; clusters can move to more larger vertical distances in the FSC96 model.

Table 5 also shows that, for most of the derived orbital parameters, the relative differences due to different potential models are smaller than those from observational errors. But for the FSC96 model, the relative differences in T_z are much larger than the uncertainties due to observational errors of input data, which indicates the major effect of the disc model of FSC96.

6 CHARACTERISTICS OF THE ORBITAL PARAMETERS

6.1 Relations among R_a–R_{GC}, R_p–R_{GC} and z_{max}–$|z|$

The left panels of Fig. 9 show the R_a versus R_{GC}, R_p versus R_{GC} and z_{max} versus $|z|$ diagrams, where $|z|$ is the current observed vertical distance from the Galactic disc. The panel of the R_a versus R_{GC}

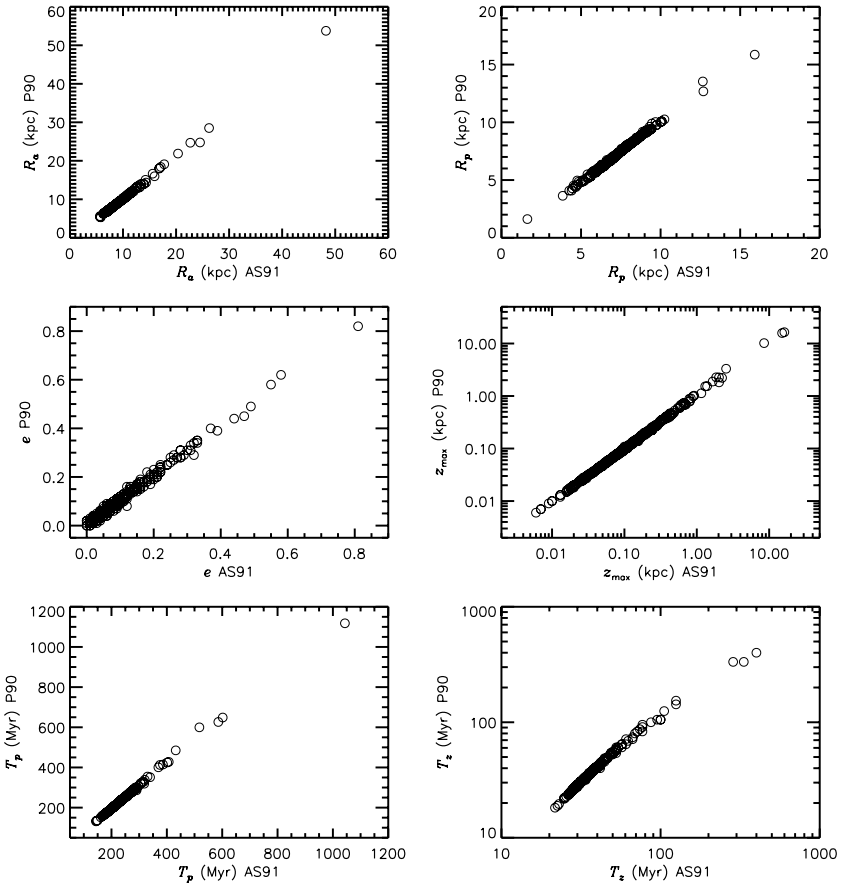

Figure 5. Comparison of derived orbital parameters with AS91 and P90 models.

diagram indicates that, for most of the clusters in the present sample, their current observed positions are very close to their apogalacticons whereas the panel of the $R_{\rm p}$ versus $R_{\rm GC}$ diagram indicates that most of the clusters are far away from their perigalacticons. The panel of the $z_{\rm max}$ versus $|z|$ diagram indicates that most of the clusters do not arrive at their maximum distances from the disc and cross the Galactic plane.

In the right-hand panels of Fig. 9, we plot the histograms of the relative differences for corresponding parameters in the left-hand panels. The top panel shows the relative difference between $R_{\rm a}$ and $R_{\rm GC}$ and indicates that, at present, about 70 per cent of the clusters are moving within only about 5 per cent distances from their apogalacticons. The median of the relative differences between $R_{\rm a}$ and $R_{\rm GC}$ is 2.0 per cent. The middle panel shows the relative difference between $R_{\rm p}$ and $R_{\rm GC}$, and indicates a significantly larger relative difference with respect to that between $R_{\rm a}$ and $R_{\rm GC}$. The median of the relative differences between $R_{\rm p}$ and $R_{\rm GC}$ is 8.1 per cent which is larger than that between $R_{\rm a}$ and $R_{\rm GC}$. The bottom panel shows the relative differences between $z_{\rm max}$ and $|z|$, and indicates very large differences between these two parameters. The median of the relative differences is 68.8 per cent. The mean time T_z for our present sample is very short, so the time for a cluster moving near its $z_{\rm max}$ is short, which is the possible reason for the large differences between the observed z and the orbital parameter $z_{\rm max}$.

For two clusters NGC 2682 and NGC 2420 whose orbital eccentricities are larger than 0.1, C94 calculated the probability of finding the clusters at the given galactocentric distances and found that the detection probability is the largest at the cluster's apogalacticon. Following C94, we also define a probability function $P(R) \propto \frac{1}{T_{\rm p}} \frac{R}{\nu(R)}$ to calculate the probability of a cluster of being observed at the galactocentric position R during the orbital period $T_{\rm p}$, where $\nu(R)$ is the cluster's velocity at R. Fig. 10 shows the probability distributions $P(R)$ for the same clusters as in Fig. 4. The filled square in Fig. 10 indicates the present observed position for each cluster. Fig. 10 shows that the detection probability $P(R)$ increases with the galactocentric distance R; the largest detection probability is at the cluster's apogalacticon. The derived probabilities for other clusters also indicate that the detection probability for a cluster at its apogalacticon is the largest one during its orbital period, which is consistent with the result of C94. Because the detection probability at the apogalacticon for a cluster is the largest during its orbital period, it is easier to find a cluster near its apogalacticon just as Fig. 9 indicates.

6.2 The radial metallicity gradient

The OCs have long been used as tracers of radial metallicity gradients in the Galactic disc. Since the early work by Janes (1979), others have found general agreement in the existence and magnitude of the trend. Most investigators have found gradients of -0.06 to -0.09 dex kpc^{-1} over a range of distances from 7 to 16 kpc from the Galactic centre (Twarog, Ashma & Anthony-Twarog 1997; Friel 1999). Recently, Friel et al. (2002) presented metallicities for a sample of 39 intermediate age and old OCs based on an updated abundance calibration of spectroscopic indices. They found a metallicity

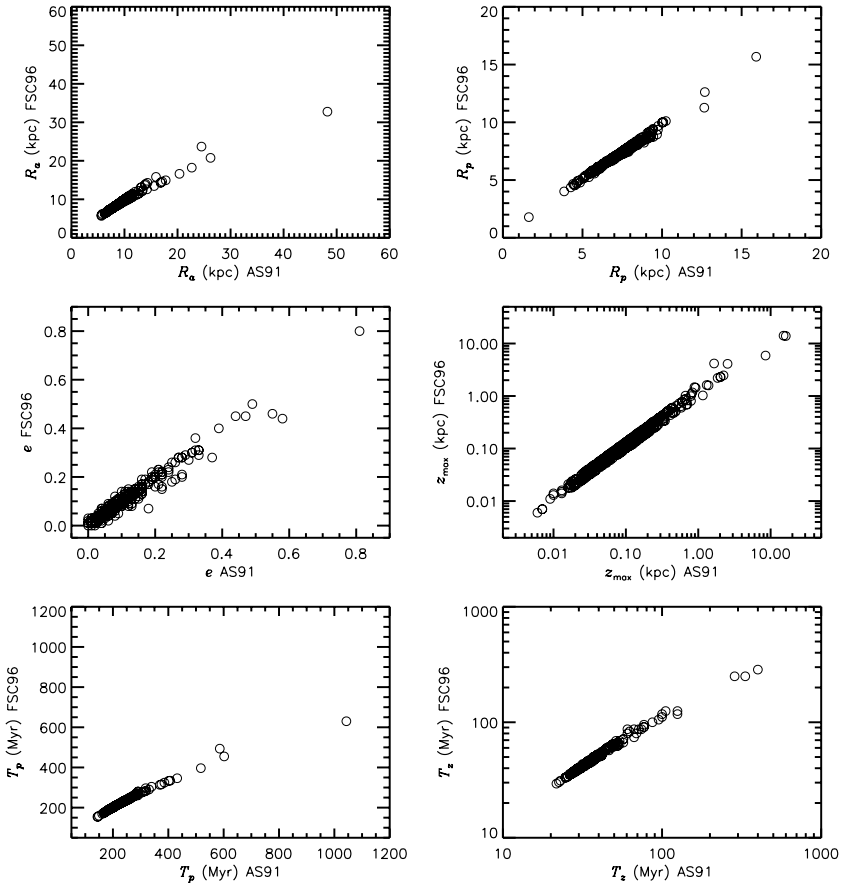

Figure 6. Comparison of derived orbital parameters with AS91 and FSC96 models.

gradient of -0.06 ± 0.01 dex kpc^{-1} over a range of galactocentric distances of 7–16 kpc. Chen et al. (2003) compiled an OCs' catalogue of 119 objects with ages, distances and metallicities available, which led to a metallicity gradient of -0.063 ± 0.008 dex kpc^{-1}, similar to the result derived by Friel et al. (2002) from a homogeneous sample.

The [Fe/H] versus current observed galactocentric distances R_{GC} diagram is plotted in the top panel of Fig. 11. 109 clusters with [Fe/H] data listed in our present sample are plotted as open circles and 48 clusters not listed in our present sample but with [Fe/H] data are plotted as plus signs. There are 12 clusters in the range of $R_{GC} > 13.5$ kpc; only three clusters are included in our present sample. Considering the observational errors in [Fe/H] and R_{GC}, we perform a linear least-square fitting to the clusters listed in our sample with $R_{GC} < 13.5$ kpc. For each cluster, we assign the typical observational uncertainty of 0.15 dex to their [Fe/H] data. The errors of R_{GC} are calculated from the data listed in Table 2. We get a gradient of -0.070 ± 0.011 dex kpc^{-1}. We also perform the same fitting to all clusters in the range of $R_{GC} < 13.5$ kpc; we get a gradient of -0.069 ± 0.008 dex kpc^{-1}. The fitted straight line for the clusters listed in our present sample within $R_{GC} < 13.5$ kpc is plotted in the same panel of Fig. 11 and the slope b of this line is also labelled.

In the most recent study, Chen et al. (2007) derived a radial metallicity gradient of -0.058 ± 0.006 dex kpc^{-1} based on a sample of 144 OCs. Our derived radial metallicity gradient of -0.07 is slightly smaller than the previous results (Friel et al. 2002; Chen et al. 2003, 2007). Based on 45 OCs with high-resolution spectroscopy, Magrini et al. (2009) found a steep metallicity gradient for clusters with $R_{GC} < 12.0$ kpc and a plateau for clusters at larger galactocentric distances. Fig. 11 indicates that the metallicity distribution of clusters with $R_{GC} > 13.5$ kpc is flat and there is no significant radial metallicity gradient within this distance range, which is consistent with the result of Magrini et al. (2009). In our present sample, only three OCs have galactocentric distances greater than 13.5 kpc (the open circles in Fig. 11). In order to diminish the effect of the small sample at large galactocentric distances, we only consider OCs with $R_{GC} < 13.5$ kpc in our present sample to derive the radial metallicity gradient. The maximum galactocentric distances of the OCs in the previous studies extend to 17 kpc and some clusters within the flat metallicity distribution were included in their samples (Friel et al. 2002; Chen et al. 2003, 2007), which is the main reason why they obtained a larger radial metallicity gradient. If we use all clusters with $R_{GC} < 17.0$ kpc, we get a gradient of -0.056 ± 0.007 dex kpc^{-1} which is consistent with the most recent result of Chen et al. (2007).

The radial metallicity gradient of the OCs provides strong constraints on the formation and evolution of the Galaxy. Detailed models of Galactic chemical evolution have been improved over the last decades and most models can reproduce the presently observed radial metallicity distribution of the Galaxy (Magrini et al. 2009, and references therein). More recently, Fu et al. (2009) considered various mechanisms including infall, star formation and delayed disc formation to find the effect of each mechanism on their derived galactic chemical evolution model. They found that using the star formation rate (SFR) of the modified Kennicutt law, their model can

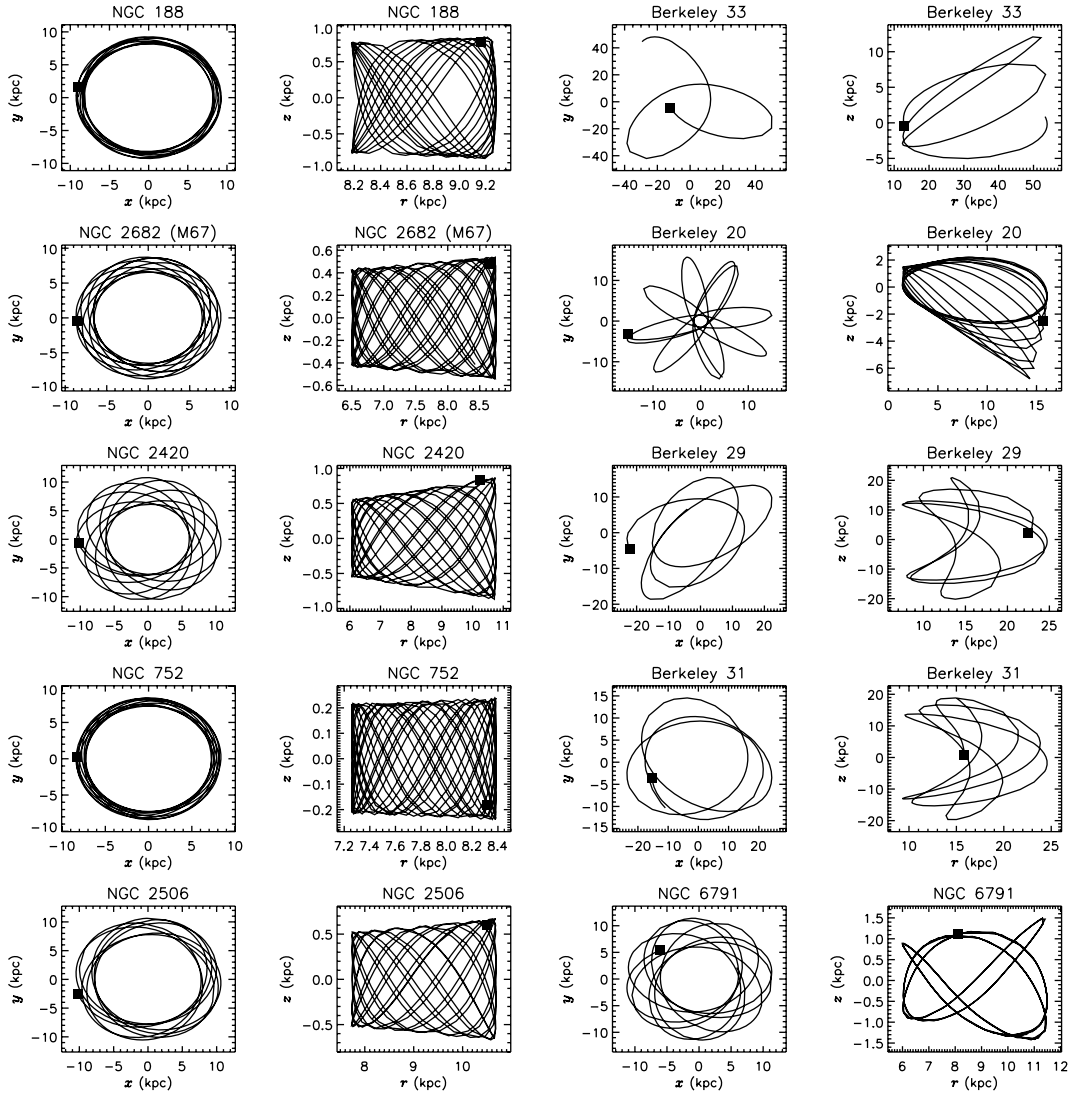

Figure 7. Meridional Galactic orbits and orbits projected on to the Galactic plane in the time interval of 2 Gyr for some OCs calculated with the P90 model. The filled square shows the present observed position for each cluster.

properly predict both the current metallicity gradient and its time evolution. But their best model also predicts that the outer disc has a steeper gradient than the inner disc, which is contrary to the result derived from OCs. Magrini et al. (2009) adopted an inside-out formation model of the Galactic disc to reproduce the radial metallicity gradient of the OCs. In their model, the infall of gas is represented by an exponential law combined with the distribution of gas in the halo. The inner regions rapidly evolve due to the higher infall and SFR, while the outer parts evolve more slowly. Their model can reproduce the main features of the metallicity gradient and the evolution of the OCs. In order to better reproduce the metallicity plateau at large galactocentric distances, an additional uniform inflow per unit disc area should be considered, but it is difficult to reconcile with the present-day radial distribution of the SFR. A sequence of merging episodes in the past history of the Galaxy would explain the outer metallicity plateau of the OCs (Magrini et al. 2009).

In our previous discussion, we have showed that the apogalacticon is the place where a cluster spends the largest fraction of its life. In the bottom panel of Fig. 11, we plot the [Fe/H] versus R_a diagram for clusters listed in our sample within $R_{GC} < 13.5$ kpc. We also perform a linear least-square fitting to the data considering the observational errors in [Fe/H] and R_a. The errors of R_a are taken from Table 3. We plot the fitted straight line in the same panel and also label the slope $b = -0.082 \pm 0.014$ dex kpc^{-1} in the panel. This result indicates that, for clusters within $R_{GC} < 13.5$ kpc, the observed metallicity gradient at present is similar to that derived from the most probable observed positions of the clusters, which is consistent with the result of C94.

6.3 Comparison of orbital eccentricities for different populations

Fig. 12 shows the histograms of orbital eccentricities for different populations: globular clusters (top-left panel), disc giants (top-right panel), disc F and G dwarf stars (lower left panel) and OCs (lower right panel). Each histogram is normalized to its maximum value in the distribution. The orbital parameters for 54 globular clusters calculated with the AS91 model are taken from A06 and A08. The orbital parameters of disc clump giants calculated with the AS91

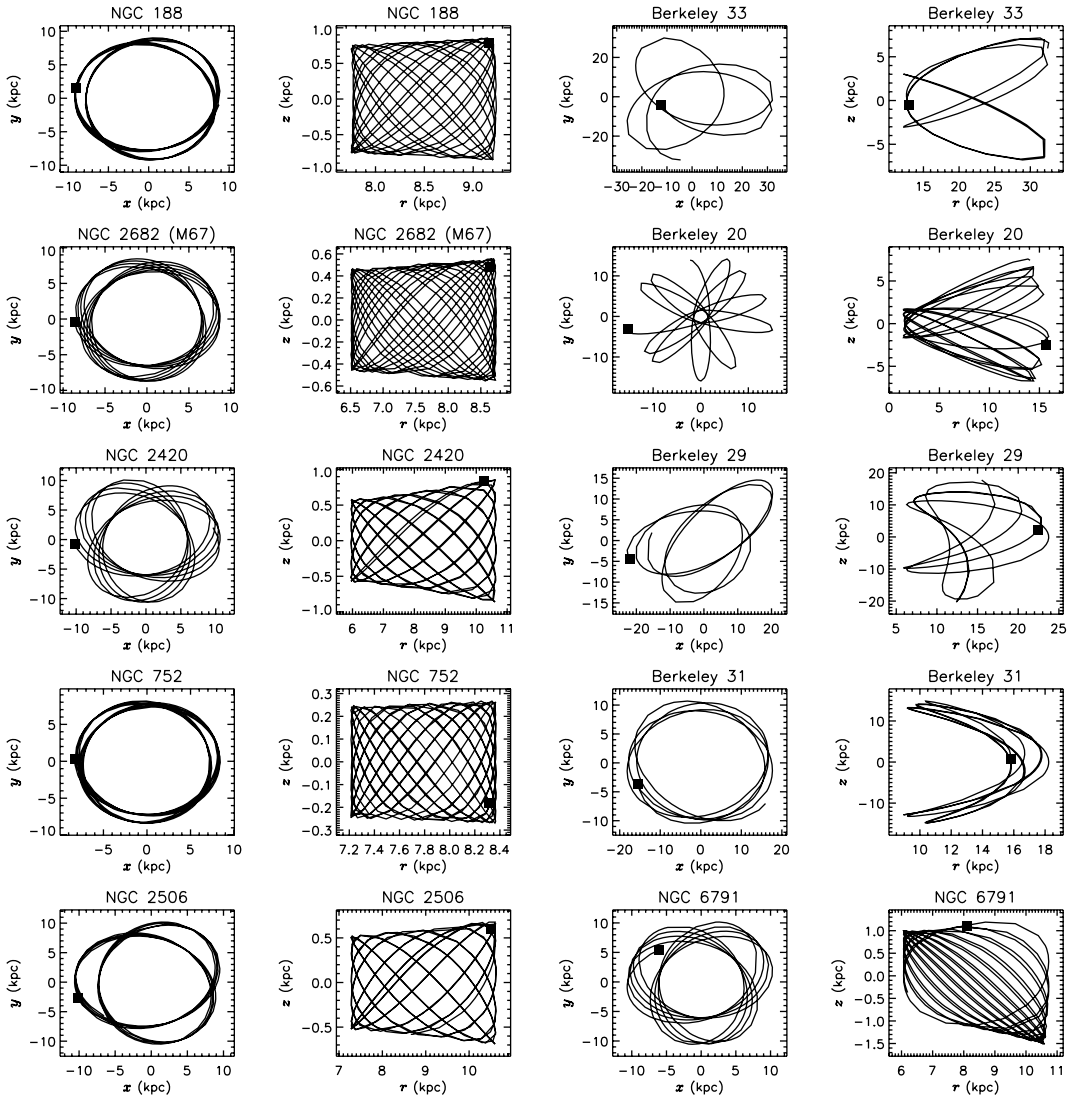

Figure 8. Meridional Galactic orbits and orbits projected on to the Galactic plane in the time interval of five times the orbital periods for some OCs calculated with the FSC96 model. The filled square shows the present observed position for each cluster.

model are taken from S08. The orbital parameters of disc F and G dwarf stars calculated with the FSC96 model are taken from N04.

Globular clusters represent the halo population which is primarily a system with a large velocity dispersion, and a wide range of orbit characteristics is expected (Dinescu et al. 1999). This is indeed what the top-left panel of Fig. 12 shows. There is a large range in the orbital eccentricities of globular clusters, which can get as low as 0.1, but, in the mean, the eccentricities are high with an average of $\sim$0.5.

S08 assigns to each star its probability of belonging to the thin disc, the thick disc, the Hercules stream and the halo based on the basis of its (U, V, W) velocity and their velocity ellipsoids. In the top-right panel of Fig. 12, we show the histograms of orbital eccentricities for stars with probabilities higher than 80 per cent of belonging to the thin disc (solid lines) and stars with probabilities higher than 80 per cent of belonging to the thick disc (dot lines). Fig. 12 indicates that no thin-disc giant has eccentricity greater than 0.3 and no thick-disc giant has eccentricity less than 0.1. The orbital eccentricities of the thin and the thick-disc giants are overlapped between 0.1 and 0.3. The average of orbital eccentricities for the thin-disc giants is $\sim$0.1 and the one for the thick-disc giants is $\sim$0.4, which is less than the average of orbital eccentricities for globular clusters.

The histogram of orbital eccentricities for disc F and G dwarf stars in the lower left panel of Fig. 12 shows that most of the stars belong to the thin disc whereas a fraction of stars belong to the thick disc. If we assume that stars with eccentricities greater than 0.3 belong to the thick disc, then the thick-disc fraction is about 3.6 per cent which is close to the value of 2.9 per cent derived by Holmberg et al. (2007) from the same sample with a different method.

The lower right panel of Fig. 12 shows the histograms of orbital eccentricities for OCs in our present sample calculated with the AS91 model (solid lines) and the FSC96 model (dot lines). The distributions of eccentricities in these two models are very similar. The distribution of orbital eccentricities for OCs is similar to that of disc F and G dwarf stars which indicates that most of the clusters belong to the thin disc and a fraction of thick-disc clusters exists in our sample. We assume the same limited value of 0.3 for orbital eccentricities to distinguish thin-disc and thick-disc clusters, and

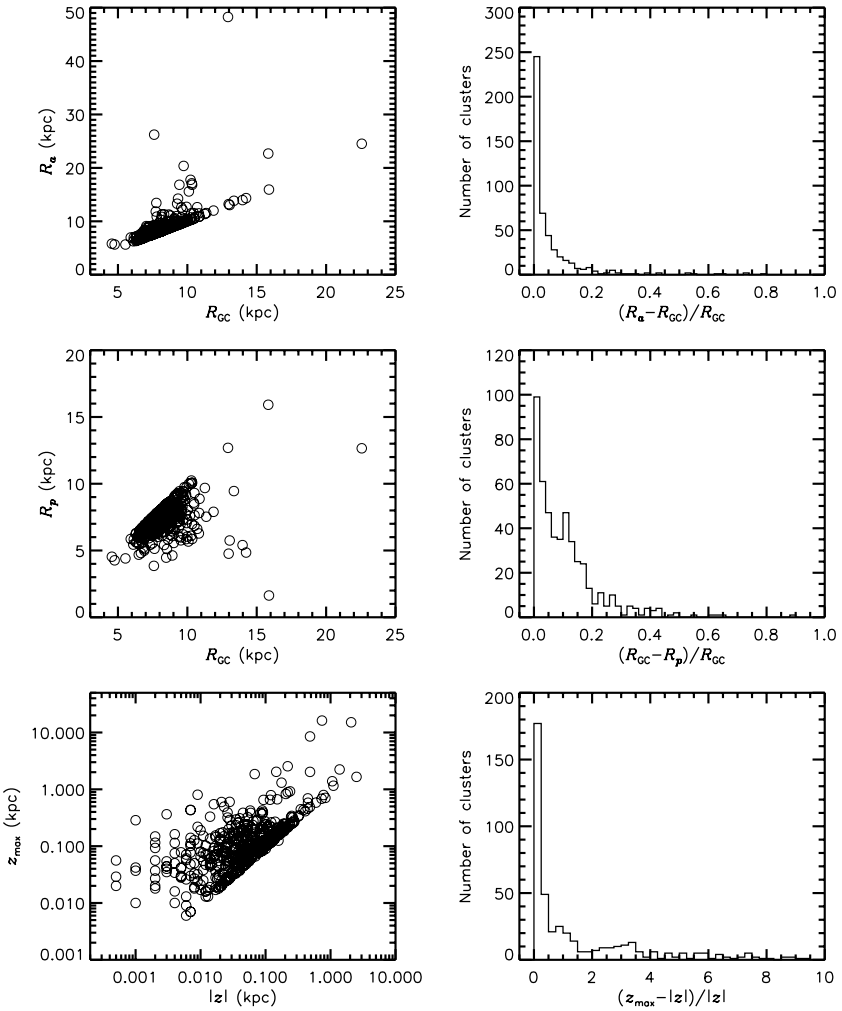

Figure 9. Relations among the orbital parameters R_a, R_p, z_{max} of OCs in our present sample and their observed data R_{GC}, $|z|$.

find that 3.7 per cent clusters in our sample are probably thick-disc clusters.

In our present sample, the z_{max} values of Berkeley 29, Berkeley 31 and Berkeley 33 are 15.1 ± 15.4, 16.2 ± 12.2 and 8.5 ± 9.3 kpc, respectively, which are much larger than those of the other clusters in the sample. The maximum of z_{max} of the other clusters is less than 3 kpc and the observed maximum of z is 2.1 kpc for Berkeley 29. The very large errors of z_{max} for these three clusters indicate that their orbits are very uncertain and more observations are needed to improve the precision of the input data for these clusters. Berkeley 20 has the maximum of $e = 0.81 \pm 0.17$ in our present sample which indicates that it is a halo cluster. But this cluster has an age of 6.0 Gyr and $[Fe/H] = -0.61 \pm 0.14$ indicating that it is a thick-disc cluster. If we adopt the limited value $e = 0.3$ with 3σ from the mean, the cluster can be identified as a member of the thick-disc population only based on orbital eccentricity e. More observations are also needed to improve the orbital parameter for this cluster.

6.4 Comparison with previous results and the open cluster complexes

There are two studies which calculated the orbits for a large samples of OCs and the orbital parameters were also derived. BKO calculated the orbits for 69 OCs and the orbital parameters R_a, R_p, e and z_{max} were also derived for these clusters. In Fig. 13, for common clusters, we compare the derived orbital parameters in the AS91 model with those derived by BKO. Fig. 13 indicates that, for most of the clusters, the derived R_a, R_p and e are consistent with those derived by BKO. The maximum difference in R_a is for NGC 2420. The radial velocity for this cluster is 73.6 km s^{-1} in our present study, but the value of 115 km s^{-1} was adopted by BKO. The large difference in radial velocity makes the large difference in R_a for NGC 2420. The maximum difference in R_p and e is for NGC 7789. A radial velocity of -64 km s^{-1} is adopted for this cluster in our study; BKO adopted the value of -32 km s^{-1}. The large difference in R_p and e for NGC 7789 is also due to the large difference in radial velocity data. For most of the OCs, the orbital parameter z_{max} in our present study are less than those derived by BKO. The systematic difference in z_{max} is due to the different disc models adopted by this study and by BKO.

Piskunov et al. (2006) calculated the orbits for a sample of 148 OCs within $d_{xy} \leq 0.85$ kpc and the mean orbital parameters are listed in their table 2: $\mu_{R_a} = 8.631$ kpc, $\mu_{R_p} = 6.706$ kpc, $\mu_e = 0.127$ and $\mu_{z_{max}} = 0.260$ kpc. For the clusters in our present sample within the same distance range, the corresponding mean orbital parameters calculated with the AS91 model are derived as $\mu_{R_a} = 8.289$ kpc, $\mu_{R_p} = 7.378$ kpc, $\mu_e = 0.059$ and $\mu_{z_{max}} = 0.084$ kpc. Because the input data for most of the clusters in this study are

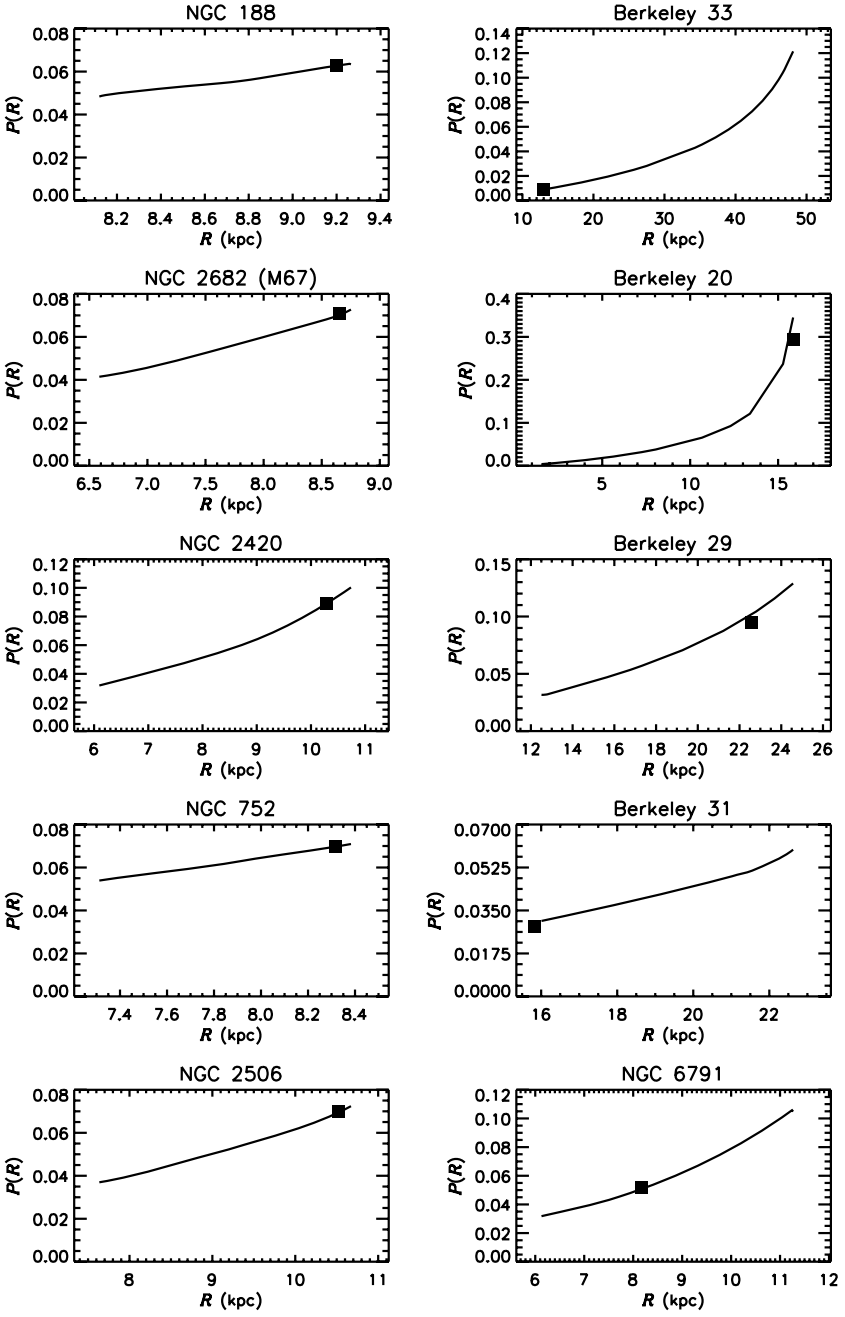

Figure 10. The detection probability distributions $P(R)$ for some OCs in our present sample. The filled square is the present observed position for each cluster.

similar to those in the study of Piskunov et al. (2006), the differences of the derived orbital parameters are mainly due to the adopted different Galactic models. Piskunov et al. (2006) used the Galactic model of Saio & Yoshii (1979); the analytic solution of the orbital parameter can be derived from their model. In comparison, the much larger disc mass in the AS91 model is responsible for the large difference in the derived value of $z_{\max}$ with respect to the other model.

Many surveys have found that the structure of the Galaxy is more complex than previously thought, and about 10 moving groups can be identified from nearby stars with heliocentric distances less than 100 pc (Bovy, Hogg & Roweis 2009). Using OCs with the projected distance on to the Galactic plane $d_{xy} \leq 0.85$ kpc from the Sun, and based on the surface density distribution and the tangential velocity distribution of those clusters, Piskunov et al. (2006) identified four OCCs. The numbers of kinematic member clusters for the four OCCs: OCC 1, OCC 2, OCC 3 and OCC 4 are 23, 27, 8 and 9, respectively (Piskunov et al. 2006). In our present sample, for the corresponding OCCs, the numbers of member clusters identified by Piskunov et al. (2006) whose orbits can be determined are 20, 13, 3 and 4.

Those OCCs were detected from their overdensity in the spatial distribution of OCs in the solar neighbourhood and the membership of the member clusters were determined only based on their tangential velocities (Piskunov et al. 2006). In Fig. 14, we use the $V_{\rm GC}$–$R_{\rm GC}$ and $z_{\max}$–e diagrams to attempt to recover those OCCs, where $V_{\rm GC}$ is the total galactocentric velocity of the cluster. The crosses in Fig. 14 represent clusters with the heliocentric distance

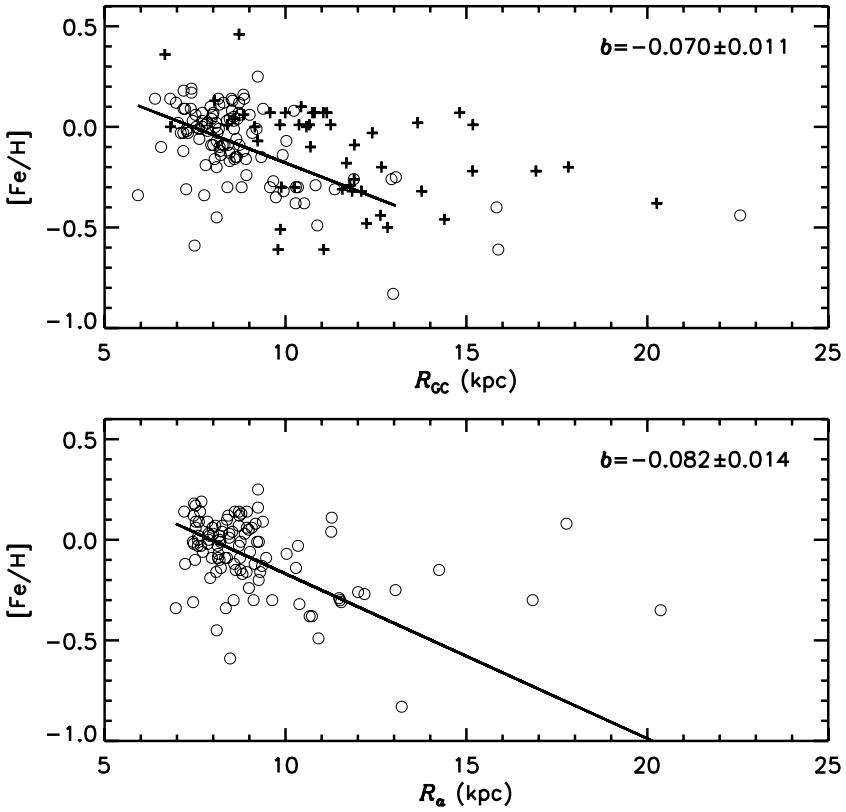

Figure 11. Metallicity gradients for OCs. Clusters included in our present sample are plotted as open circles and clusters not included in our present sample but with [Fe/H] data are plotted as plus signs. Top panel: the metallicity gradient of OCs is derived based on the currently observed galactocentric distances of OCs R_{GC}; bottom panel: the metallicity gradient of OCs is derived based on apogalactic distances R_a. The straight lines are the best-fitting results of the metallicity gradients for OCs in our present sample with $R_{GC} < 13.5$ kpc and the slopes b for each line, that is the gradients, are labelled in each panel.

less than 1.3 kpc and the open circles represent member clusters in each OCC. In the panels of OCC 1, the open circles represent member clusters with an age less than 30 Myr and triangles represent member clusters with an age between 30 and 80 Myr. There are 18 member clusters in OCC 1 whose age data are available. The V_{GC}–R_{GC} diagram of OOC 1 indicates that six clusters with an age less 30 Myr and four clusters with an age greater than 30 Myr distribute in a small region with $212 < V_{GC} < 219$ km s^{-1} and $8.0 < R_{GC} < 8.5$ kpc; these clusters can be considered as kinematic members of OCC 1. But in the z_{max}–e diagram of OCC 1, it is difficult to identify any clustering of these member clusters. We could only determine the orbits of 50 per cent of the assumed members of OCC 2. Most of the member clusters of OCC 2 have an age between 200 and 400 Myr. The panels of OCC 2 indicate that we cannot detect any clustering of the member clusters in the V_{GC}–R_{GC} and z_{max}–e diagrams. OCCs 3 and 4 only include a few of the member clusters; the panels of these two OCCs indicate that no clustering of the member clusters can be identified. Fig. 14 indicates that only young OCCs can be identified in the V_{GC}–R_{GC} diagram, and it is difficult to detect clustering in OCs with the z_{max}–e diagram.

More recently, using the radial velocity, proper motion, inclination and Galactic latitude of 341 OCs with an age less than 100 Myr and within 2.5 kpc from the Sun, de la Fuente Marcos & de la Fuente Marcos (2008) studied the clustering in those clusters. Most of the member clusters in the closest OCC detected by de la Fuente Marcos & de la Fuente Marcos (2008) have an age less than 30 Myr, which is consistent with that we have found in the V_{GC}–R_{GC} diagram of OCC 1. de la Fuente Marcos & de la Fuente Marcos (2008) pointed out that 20 Myr is the characteristic time-scale of an OCC; after this time-scale, the complex may no longer be recognizable in the space of the orbital elements as the majority of its members have evaporated. It is only in the context of corotation resonances or mergers that the non-genetically related dynamical groups of old OCs can be detected in the Galactic disc.

7 SUMMARY AND CONCLUSIONS

We have presented a sample of 488 OCs whose distances, radial velocities and absolute proper motions are used to derive their orbits in the Galaxy. The kinematical and the orbital characteristics of this sample are analysed. The main results are listed as follows.

(i) For OCs with errors in the spatial velocities less than 20 km s^{-1} in our present sample, the velocity ellipsoids are derived as $(\sigma_U, \sigma_V, \sigma_W) = (28.7, 15.8, 11.0)$ km s^{-1}. The ages for most of the clusters in our present sample are less than 500 Myr, and this sample represents a young thin-disc population. The velocity dispersions of OCs in the three velocity components increase with the age of the cluster subsample, which indicates the continuous heating of the disc (N04).

(ii) The orbits of OCs are calculated with three Galactic gravitational potential models. Considering the intrinsic variation of orbital parameters and the effects of observational uncertainties, the errors for the derived orbital parameters are determined in a Monte Carlo fashion. The major errors come from the observational uncertainties of the input data and are mainly affected by the errors in the

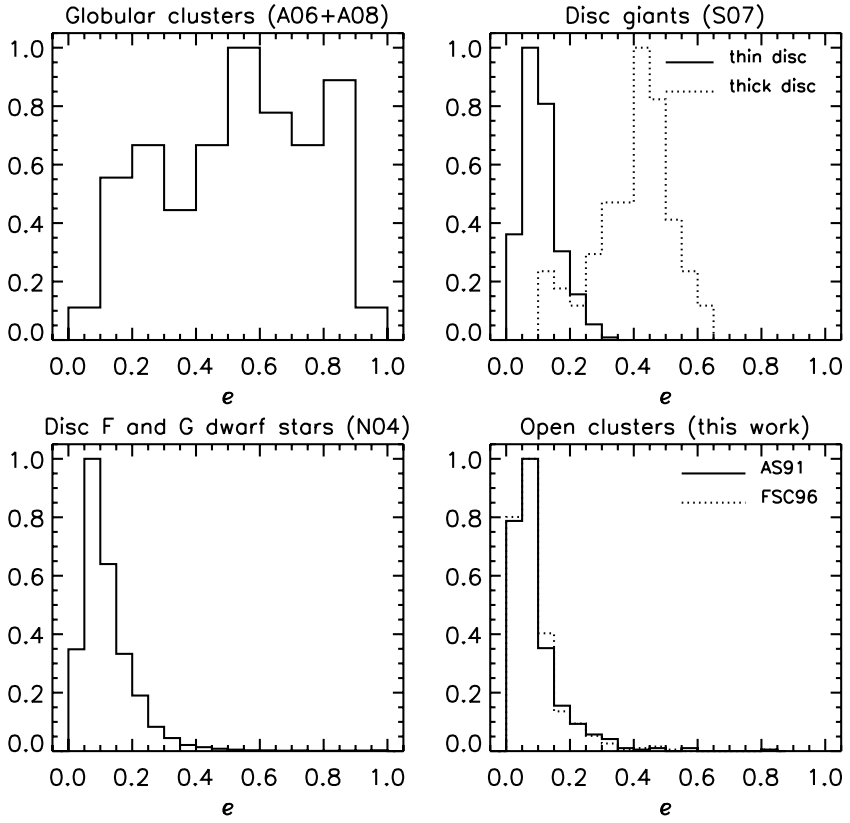

Figure 12. Comparison of orbital eccentricities e for different populations: globular clusters (A06+A08), disc giants (S08), disc F and G dwarf stars (N04), and OCs (this work).

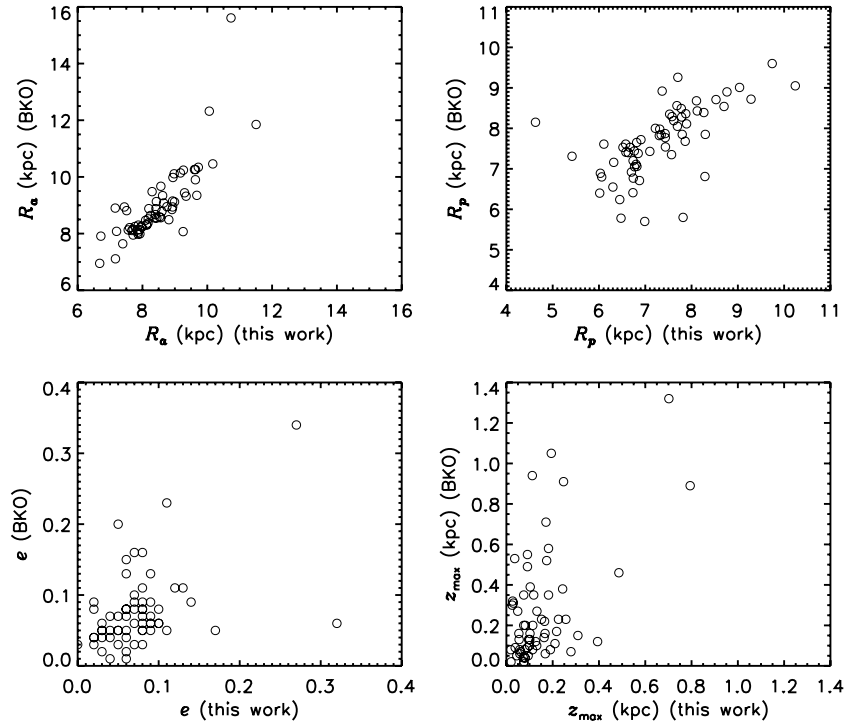

Figure 13. The derived orbital parameters R_a, R_p, e and z_{max} with the AS91 model in this work are compared with those derived by BKO.

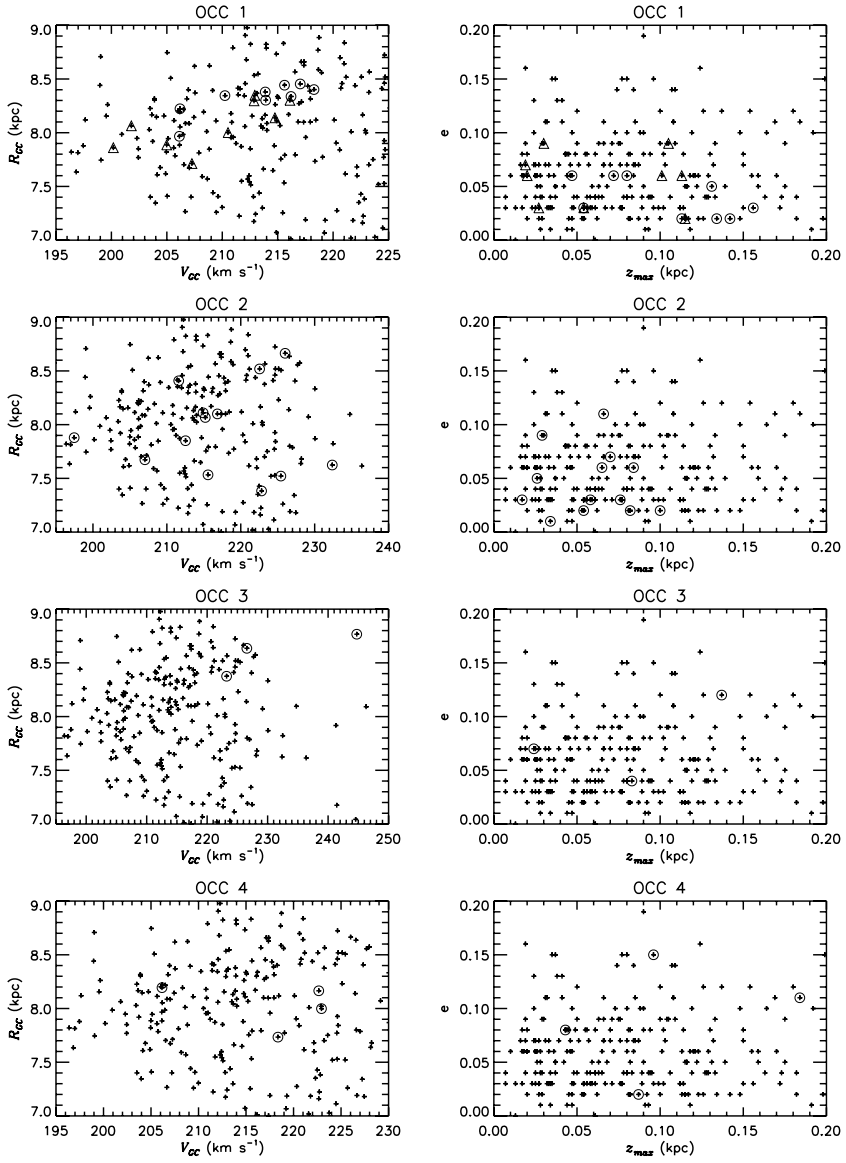

Figure 14. The orbital parameter distributions of four OCCs identified by Piskunov et al. (2006). The open circles are member clusters for each OCC and crosses are clusters with heliocentric distance less than 1.3 kpc. In the panels of OCC 1, the open circles represent member clusters younger than 30 Myr and the triangles represent member clusters with an age between 30 and 80 Myr.

distance data. The observational uncertainties mainly affect the derived orbital eccentricities e and the maximum distances above the Galactic disc $z_{\max}$.

(iii) The total masses within a given distance range for different Galactic models can affect the derived orbital parameter $R_{\rm a}$ and the orbital period $T_{\rm p}$. The disc models for different Galactic models mainly affect the vertical movement of clusters and change the derived $z_{\max}$ and T_z. The uncertainties in the derived orbital parameters caused by different models are smaller than those caused by observational errors in the input data.

(iv) The detection probability for a cluster at the given galactocentric distance is calculated and the largest detection probability is at the cluster's apogalacticon. For most of the OCs in our present sample, their present observed positions are very close to their apogalacticons. The mean of the orbital period for OCs is about seven times longer than the time for clusters crossing the Galactic plane.

(v) Based on the presently observed galactocentric distances, the radial metallicity gradient for clusters with $R_{\rm GC} < 13.5$ kpc is derived with a slope -0.070 ± 0.011 dex kpc^{-1}, which is consistent with the previous studies (Friel et al. 2002; Chen et al. 2003). The derived radial metallicity gradient based on apogalactic distances for the same sample is -0.082 ± 0.014 dex kpc^{-1}.

(vi) The orbital eccentricities e for different populations: globular clusters, disc giants, disc F and G dwarf stars, and OCs are compared. The orbital eccentricities for globular clusters occupy a large range with a mean of $\sim$0.5. The mean of orbital eccentricities for the thick-disc giants is $\sim$0.4 which is bigger than the mean of $\sim$0.1 for the thin-disc giants, F and G dwarfs, and OCs. There are about 3.7 per cent clusters in our sample belonging to the thick disc.

(vii) Using the $V_{\rm GC}$–$R_{\rm GC}$ diagram, only one OCC could be identified and most of its members are younger than 30 Myr. We find it difficult to detect any OCCs in the $z_{\max}$–e diagram.

ACKNOWLEDGMENTS

We are grateful to an anonymous referee for a particularly constructive and prompt report. This work has been supported in part by the National Natural Science Foundation of China, no.10633020, 10603006, 10778720, 10873016 and 10803007, and by the National Basic Research Program of China (973 Program) no. 2007CB815403. Z-YW acknowledges support from the Knowledge Innovation Program of the Chinese Academy of Sciences. This research has made use of the WEBDA data base, operated at the Institute for Astronomy of the University of Vienna.

REFERENCES

Alessi B. S., Moitinho A., Dias W. S., 2003, A&A, 410, 565
Allen C., Martos M. A., 1988, Rev. Mex. Astron. Astrofis., 16, 25
Allen C., Santillán A., 1991, Rev. Mex. Astron. Astrofis., 22, 255 (AS91)
Allen C., Moreno E., Pichardo B., 2006, ApJ, 652, 1150 (A06)
Allen C., Moreno E., Pichardo B., 2008, ApJ, 674, 237 (A08)
Barbier-Brossat M., Figon P., 2000, A&AS, 142, 217
Barkhatova K. A., Kutuzov S. A., Osipkov L. P., 1987, SvA, 31, 501 (BKO)
Barkhatova K. A., Osipkov L. P., Kutuzov S. A., 1989, SvA, 33, 596
Baumgardt H., Dettbarn C., Wielen R., 2000, A&AS, 146, 251
Bergond G., Leon S., Guibert J., 2001, A&A, 377, 462
Bonatto C., Kerber L. O., Bica E., Santiago B. X., 2006, A&A, 446, 121
Bovy J., Hogg D. W., Roweis S. T., 2009, ApJ, 700, 1794
Carraro G., Chiosi C., 1994, A&A, 288, 751 (C94)
Chen L., Hou J. L., Wang J. J., 2003, AJ, 125, 1397
Chen L., Hou J. L., Zhao J. L., de Grijs R., 2007, in Jin W. J., Platais I., Perryman M. A. C., eds, Proc. IAU Symp. 248, A Giant Step: from Milli- to Micro-Arcsecond Astrometry. Kluwer, Dordrecht, p. 433
de la Fuente Marcos R., de la Fuente Marcos C., 2008, ApJ, 672, 342
de Oliveira M. R., Fausti A., Bica E., Dottori H., 2002, A&A, 390, 103
Dehnen W., Binney J., 1998, MNRAS, 298, 387
Dias W. S., Lépine J. R. D., 2005, ApJ, 629, 825
Dias W. S., Lépine J. R. D., Alessi B. S., 2001, A&A, 376, 441
Dias W. S., Alessi B. S., Moitinho A., Lépine J. R. D., 2002a, A&A, 389, 871 (DAML)
Dias W. S., Lépine J. R. D., Alessi B. S., 2002b, A&A, 388, 168
Dias W. S., Assafin M., Flório V., Alessi B. S., Líbero V., 2006, A&A, 446, 949
Dinescu D. I., Girard T. M., van Altena W. F., 1999, AJ, 117, 1792
Efremov Y. N., 1978, Sov. Astron. Lett., 4, 66
Éigenson A. M., Yatsyk O. S., 1988, SvA, 32, 168
ESA, 1997, The Hipparcos and Tycho Catalogues, ESA SP-1200
Finlay J., Noriega-Crespo A., Friel E. D., Cudworth K., 1995, BAAS, 27, 1437
Flynn C., Sommer-Larsen J., Christensen P. R., 1996, MNRAS, 281, 1027 (FSC96)
Friel E. D., 1995, ARA&A, 33, 381
Friel E. D., 1999, Ap&SS, 265, 271
Friel E. D., Janes K. A., Tavarez M., Scott J., Katsanis R., Lotz J., Hong L., Miller N., 2002, AJ, 124, 2693
Frinchaboy P. M., Majewski S. R., 2008, ApJ, 136, 118
Fu J., Hou J. L., Yin J., Chang R. X., 2009, ApJ, 696, 668
Holmberg J., Nordström B., Andersen J., 2007, A&A, 475, 519
Høg E. et al., 2000, A&A, 355, L27
Janes K. A., 1979, ApJS, 39, 135
Janes K. A., Tilley C., Lyngå G., 1988, AJ, 95, 771
Johnson D. R. H., Soderblom D. R., 1987, AJ, 93, 864
Jørgensen B. R., Lindegren L., 2005, A&A, 436, 127
Keenan D. W., Innanen K. A., House F. C., 1973, AJ, 78, 173
Kerr F. J., Lynden-Bell D., 1986, MNRAS, 221, 1023
Kharchenko N. V., 2001, Kinematics Phys. Celest. Bodies, 17, 409
Kharchenko N. V., Piskunov A. E., 2006, Astron. Astrophys. Trans., 25, 177
Kharchenko N. V., Pakulyak L. K., Piskunov A. E., 2003, Astron. Rep., 47, 263
Kharchenko N. V., Piskunov A. E., Röser S., Schilbach E., Scholz R.-D., 2005, A&A, 438, 1163 (K05)
Kharchenko N. V., Scholz R.-D., Piskunov A. E., Röser S., Schilbach E., 2007, Astron. Notes, 328, 889
Kovalevsky J. et al., 1997, A&A, 323, 620
Lada C. J., Lada E. A., 2003, ARA&A, 41, 57
Lépine J. R. D., Dias W. S., Mishurov Y., 2008, MNRAS, 386, 2081
Loktin A. V., Beshenov G. V., 2003, Astron. Rep., 47, 6
Lyngå G., 1982, A&A, 109, 213
Lyngå G., 1987, Catalogue of Open Cluster Data, 5th edn. CDS, Strasbourg
Lyngå G., Palouš J., 1987, A&A, 188, 35
Magrini L., Sestito P., Randich S., Galli D., 2009, A&A, 494, 95
Mermilliod J. C., Mayor M., Udry S., 2008, A&A, 485, 303
Miyamoto M., Nagai R., 1975, PASJ, 27, 533
Nordström B. et al., 2004, A&A, 418, 989 (N04)
Odenkirchen M., Brosche P., 1992, Astron. Nachr., 313, 69
Odenkirchen M., Brosche P., Geffert M., Tucholke H.-J., 1997, New Astron., 2, 477
Paczyński B., 1990, ApJ, 348, 485 (P90)
Paunzen E., Netopil M., 2006, MNRAS, 371, 1641
Piskunov A. E., Kharchenko N. V., Röser S., Schilbach E., Scholz R.-D., 2006, A&A, 445, 545
Platais I., Kozhurina-Platais V., van Leeuwen F., 1998, AJ, 116, 2423
Plummer H. C., 1911, MNRAS, 71, 460
Press W. H., Teukolsky S. A., Vetterling W. T., Flannery B. P., 1992, Numerical Recipes in Fortran: The Art of Scientific Computing, 2nd edn. Cambridge Univ. Press, Cambridge
Reid M. J., 1993, ARA&A, 31, 345
Röser S., Kharchenko N. V., Piskunov A. E., Schilbach E., Scholz R.-D., 2007, in Vesperini E., Giersz M., Sills A., eds, Proc. IAU Symp. 246, Dynamical Evolution of Dense Stellar Systems. Kluwer, Dordrecht, p. 115
Saio H., Yoshii Y., 1979, PASP, 91, 553
Seabroke G. M., Gilmore G., 2007, MNRAS, 380, 1348
Soubiran C., Odenkirchen M., Le Campion J.-F., 2000, A&A, 357, 484
Soubiran C., Bienaymé O., Mishenina T. V., Kovtyukh V. V., 2008, A&A, 480, 91 (S08)
Twarog B. A., Ashma K. M., Anthony-Twarog B. J., 1997, AJ, 114, 2556
Urban S. E., Wycoff G. L., Makarov V. V., 2000, AJ, 120, 501
van Leeuwen F., 2007, A&A, 474, 653
van Leeuwen F., 2008, Hipparcos, the New Reduction of the Raw Data. Springer, Dordrecht
Wu Z. Y., Tian K. P., Balaguer-Núñez L., Jordi C., Zhao L., Guibert J., 2002, A&A, 381, 464
Zacharias N., Urban S. E., Zacharias M. I., Wycoff G. L., Hall O. M., Monet D. G., Rafferty T. J., 2004, AJ, 127, 3043

SUPPORTING INFORMATION

Additional Supporting Information may be found in the online version of this article:

Table 1. The observed data of 488 OCs in our sample.
Table 2. The present positions and velocities of 488 OCs in our sample.
Table 4. The orbital parameters and their errors of 488 OCs in our sample calculated with the AS91 model.

Please note: Wiley-Blackwell are not responsible for the content or functionality of any supporting materials supplied by the authors. Any queries (other than missing material) should be directed to the corresponding author for the article.

This paper has been typeset from a TEX/LATEX file prepared by the author.